Activation of Rac by Asef2 promotes myosin II-dependent contractility to inhibit cell migration on type I collagen

Léolène Jean[1], Devi Majumdar[1], Mingjian Shi[1], Louis E. Hinkle[1], Nicole L. Diggins[1], Mingfang Ao[1], Joshua A. Broussard[1], J. Corey Evans[1], David P. Choma[1,2] and Donna J. Webb[1,3,*]

[1]Department of Biological Sciences and Vanderbilt Kennedy Center for Research on Human Development, Nashville, TN 37203, USA
[2]Department of Nephrology, Vanderbilt University, Nashville, TN 37235, USA
[3]Department of Cancer Biology, Vanderbilt University, Nashville, TN 37235, USA
*Author for correspondence (donna.webb@vanderbilt.edu)

Accepted 23 September 2013
Journal of Cell Science 126, 5585–5597

doi: 10.1242/jcs.131060

Summary

Non-muscle myosin II (MyoII) contractility is central to the regulation of numerous cellular processes, including migration. Rho is a well-characterized modulator of actomyosin contractility, but the function of other GTPases, such as Rac, in regulating contractility is currently not well understood. Here, we show that activation of Rac by the guanine nucleotide exchange factor Asef2 (also known as SPATA13) impairs migration on type I collagen through a MyoII-dependent mechanism that enhances contractility. Knockdown of endogenous Rac or treatment of cells with a Rac-specific inhibitor decreases the amount of active MyoII, as determined by serine 19 (S19) phosphorylation, and negates the Asef2-promoted increase in contractility. Moreover, treatment of cells with blebbistatin, which inhibits MyoII activity, abolishes the Asef2-mediated effect on migration. In addition, Asef2 slows the turnover of adhesions in protrusive regions of cells by promoting large mature adhesions, which has been linked to actomyosin contractility, with increased amounts of active β1 integrin. Hence, our data reveal a new role for Rac activation, promoted by Asef2, in modulating actomyosin contractility, which is important for regulating cell migration and adhesion dynamics.

Key words: Rho GTPases, Adhesion dynamics, Actomyosin, Guanine nucleotide exchange factor, β1 integrin, Asef2, SPATA13

Introduction

Cell migration is vital for embryonic development and in maintaining homeostasis in the adult (Vicente-Manzanares and Horwitz, 2011). Migration also plays a central role in pathological disorders, such as atherosclerosis, arthritis and cancer. Therefore, identifying key molecular mechanisms that regulate migration is important for developing new therapeutic approaches for treating these disorders. Cell migration comprises several underlying processes that include establishment of front-back polarity, extension of leading edge protrusions, formation of cell–matrix adhesions, translocation of the cell body and retraction of the cell rear (Lauffenburger and Horwitz, 1996; Vicente-Manzanares et al., 2005). The formation of integrin-based adhesions, which link the actin cytoskeleton to the extracellular matrix (ECM), stabilize leading edge protrusions and generate traction forces on the ECM to propel cell movement (Beningo et al., 2001; Gardel et al., 2008). These nascent adhesions can continue to grow and mature into large focal adhesions, or they can subsequently disassemble to allow for sustained migration (Laukaitis et al., 2001; Webb et al., 2004). The continuous assembly and disassembly of adhesions, termed adhesion turnover, is crucial for cell migration (Webb et al., 2004).

MyoII is an actin motor protein that is emerging as a key modulator of cell migration through its ability to regulate underlying processes. MyoII is important for stabilizing leading edge protrusions and maintaining polarity (Lo et al., 2004). Moreover, MyoII is essential for the maturation of adhesions as well as retraction of the cell rear (Choi et al., 2008; Vicente-Manzanares et al., 2007). Structurally, MyoII is composed of two heavy chains (MHC) as well as two essential (ELC) and two regulatory (RLC) light chains. Each MHC contains an N-terminal head domain, a neck region, and a C-terminal α-helical rod domain (Wang et al., 2011). The head domains, which contain the motor region, bind to actin and allow MyoII to move along actin filaments by coupling the hydrolysis of ATP to conformational changes. The rod domains can associate with other MyoII rod domains to form bipolar filaments. These bipolar filaments generate contraction by sliding actin filaments relative to one another, which is a major cellular function of MyoII. The activity and function of MyoII is regulated by phosphorylation within the RLC (Adelstein and Conti, 1975; Scholey et al., 1980). Phosphorylation of serine 19 activates the motor domain of MyoII and drives actomyosin contractility (Adelstein and Conti, 1975; Ikebe, 1989). Additional phosphorylation on another residue, threonine 18, further enhances myosin ATPase activity (Ikebe, 1989).

The Rho family of GTPases, which includes Rho, Rac and Cdc42, are molecular switches that exist in two interconvertible forms: a GDP-bound form (inactive) and a GTP-bound form (active) (Ridley et al., 2003). Active GTPases interact with their specific downstream targets to modulate cell migration, actin

polymerization, MyoII contraction and adhesion dynamics (Huttenlocher and Horwitz, 2011; Ridley, 2001; Ridley et al., 2003). Rac and Cdc42 regulate the formation of protrusive actin-based structures, lamellipodia and filopodia, respectively, whereas Rho is thought to stabilize lamellipodial protrusions (Nobes and Hall, 1995; Ridley and Hall, 1992). Rac promotes the assembly of nascent adhesions near the cell periphery, whereas Rho activity induces adhesion maturation (Chrzanowska-Wodnicka and Burridge, 1996; Ridley and Hall, 1992; Rottner et al., 1999). Rho activity also stimulates the formation of stress fibers, which are contractile F-actin bundles, and promotes actomyosin contractility (Chrzanowska-Wodnicka and Burridge, 1996; Katoh et al., 2001; Ridley and Hall, 1992). However, little is currently known about the function of the other Rho GTPases, including Rac, in modulating actomyosin contraction.

The activation of Rho GTPases is regulated by guanine nucleotide exchange factors (GEFs), which facilitate the release of GDP from the GTPases, thus promoting the binding of GTP. Asef2 (also known as SPATA13) is a recently identified GEF known to activate both Rac and Cdc42 (Hamann et al., 2007; Kawasaki et al., 2007). Asef2 comprises four domains, including an N-terminal adenomatous polyposis coli (APC)-binding region (ABR), an adjacent Src homology 3 (SH3) domain, a central Dbl homology (DH) domain that binds GTPases and is necessary for its catalytic function, and a pleckstrin homology (PH) domain, which facilitates membrane targeting (Hamann et al., 2007; Kawasaki et al., 2007). Binding of the tumor suppressor APC to the ABR region has been shown to stimulate the GEF activity of Asef2 by releasing it from an auto-inhibited state, where the C-terminus is bound to the ABR-SH3 domains (Hamann et al., 2007). Asef2 has been implicated in the regulation of cell migration (Bristow et al., 2009; Sagara et al., 2009), but its role in modulating this process is not well understood.

In this study, we demonstrate that Asef2 inhibits cell migration on type I collagen by a Rac- and MyoII-dependent mechanism. Asef2 promotes the activation of Rac, which subsequently stimulates MyoII contractility. In addition, Asef2 slows adhesion turnover and induces large mature adhesions. Therefore, Asef2 modulation of Rac- and MyoII-dependent contractility is likely to regulate cell migration by affecting underlying migratory processes such as adhesion turnover.

Results

Asef2 inhibits cell migration on type I collagen

We have previously shown that Asef2 promotes cell migration when cells are plated on fibronectin (Bristow et al., 2009). Indeed, in our previous study, the migration speed of HT1080 cells stably expressing GFP–Asef2 was increased 1.6-fold compared to control cells stably expressing GFP. In this study, to further investigate the role of Asef2 in regulating cell migration, we plated GFP–Asef2 and GFP stably expressing cells on type I collagen. These cells express low levels of GFP–Asef2 (less than 3-fold over endogenous) (Bristow et al., 2009). Intriguingly, GFP–Asef2 cells, plated on type I collagen, migrated significantly more slowly than GFP control cells (Fig. 1A; supplementary material Movies 1, 2), suggesting that Asef2 impairs migration on type I collagen. Given that these results were surprising, we performed side-by-side migration experiments with GFP and GFP–Asef2 stably expressing cells plated on fibronectin or type I collagen. Consistent with our previous results, GFP–Asef2 promoted migration on fibronectin, but inhibited migration on type I collagen, indicating that Asef2 differentially affects migration on these substrates (supplementary material Fig. S1A). We continued to probe the function of Asef2 in regulating migration on type I collagen by transiently transfecting wild-type HT1080 cells with GFP–Asef2 or GFP as a control. As with the stable cells, expression of GFP–Asef2 resulted in a decrease in migration speed as compared to that observed with GFP-expressing cells (supplementary material Fig. S1B). We then examined the effect of Asef2 on migration on type I collagen in another cell type by generating MDA-MB-231 cells that stably expressed GFP–Asef2 or GFP as a control. As with HT1080 cells, stable expression of GFP–Asef2 in MDA-MB-231 led to a significant reduction in migration speed as compared to that observed with GFP-expressing cells (supplementary material Fig. S2A), suggesting Asef2 inhibits migration on type I collagen.

We further probed the role of Asef2 in regulating migration on type I collagen by knocking down endogenous expression of the protein using two short hairpin RNA (shRNA) constructs. Although these shRNAs had previously been shown to be effective (Bristow et al., 2009), we confirmed their ability to knockdown Asef2. When wild-type HT1080 cells were transfected with Asef2 shRNA 1 or Asef2 shRNA 2, endogenous expression of Asef2 was decreased by ~65% compared with empty pSUPER vector or a non-targeting shRNA (NT shRNA) (Fig. 1B). Transfection of HT1080 cells with the two Asef2 shRNAs resulted in a 1.3-fold increase in migration speed compared to that observed with cells transfected with pSUPER or NT shRNA (Fig. 1C; supplementary material Movies 3, 4), demonstrating that knockdown of endogenous Asef2 enhances migration on type I collagen. Collectively, our results suggest an interesting new role for Asef2 in regulating migration on type I collagen.

Rac activity is enhanced by Asef2

We next investigated the mechanism by which Asef2 impairs migration on type I collagen. In initial experiments, we examined the effect of Asef2 on the activity of the Rho family GTPases Rac, Cdc42 and Rho using a pulldown assay. In this assay, GFP and GFP–Asef2 cells were plated on type I collagen, and GST-tagged binding domains from effectors were used to detect the active forms of these small GTPases from cell lysates. Interestingly, GFP–Asef2 expression did not significantly affect the level of active Cdc42 or Rho (Fig. 2A). In contrast, the amount of active Rac was increased ~1.8-fold in GFP–Asef2 cells compared to GFP controls (Fig. 2A). Moreover, knockdown of endogenous Asef2 in wild-type HT1080 cells by transfection with Asef2 shRNA 1 caused a decrease in Rac activity compared to that observed with cells transfected with NT shRNA (Fig. 2B). Taken together, these results suggest that Asef2 promotes the activation of Rac, but not Cdc42 and Rho, when cells are plated on type I collagen.

To further demonstrate that Asef2 increases Rac activity, we used a Raichu-Rac fluorescence resonance energy transfer (FRET) probe. Raichu-Rac is composed of yellow fluorescent protein (YFP), the p21-binding domain (PBD) from the Rac effector p21-activated kinase (PAK), Rac, and cyan fluorescent protein (CFP) (Itoh et al., 2002). Upon activation, Rac binds to PBD, which brings YFP and CFP in close enough proximity to undergo FRET (Itoh et al., 2002). To perform acceptor

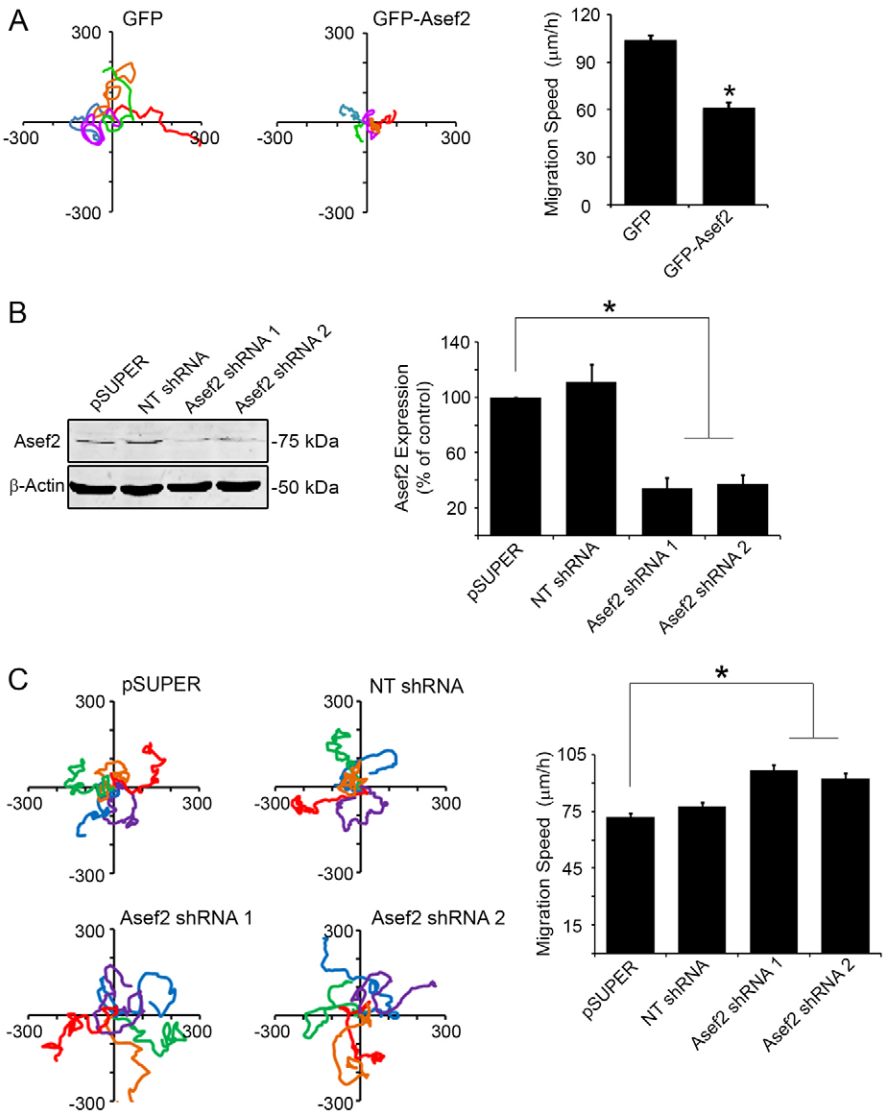

Fig. 1. Asef2 impairs cell migration on type I collagen. (A) GFP and GFP–Asef2 stably expressing HT1080 cells were plated on tissue culture dishes coated with type I collagen and imaged using time-lapse microscopy. The migration paths of individual cells were tracked and analyzed. Left, Rose plots of the migration tracks for five cells. Right, quantification of the migration speed for GFP and GFP–Asef2 cells. Error bars represent the s.e.m. for 59–63 cells from three independent experiments. *$P<0.0001$. (B) Left, wild-type HT1080 cells were transfected with empty pSUPER vector, a non-targeting shRNA (NT shRNA), or Asef2 shRNAs. Cell lysates were immunoblotted for Asef2 to determine endogenous expression of this protein and for β-actin as a loading control. Right, quantification of the amount of endogenous Asef2 in cells transfected with the indicated constructs. Error bars represent the s.e.m. from five independent experiments. *$P<0.0001$. (C) Wild-type HT1080 cells were transfected with empty pSUPER vector, a NT shRNA or Asef2 shRNAs and used in migration assays 3 days later. Left, Rose plots of migration tracks for cells transfected with these constructs. Right, quantification of the migration speed for cells transfected with empty pSUPER vector, a NT shRNA, or Asef2 shRNAs. Error bars represent the s.e.m. for at least 40 cells from three independent experiments. *$P<0.0001$.

photo-bleaching FRET, we expressed the Raichu-Rac probe and either mCherry–Asef2 or mCherry as a control in HT1080 cells and photo-bleached a region of interest (ROI) with a 514 nm laser. With acceptor photo-bleaching, when YFP (FRET acceptor) is photo-bleached, the intensity of CFP (FRET donor) increases if FRET occurs. YFP images, taken pre- and post-bleaching, demonstrated that YFP was effectively photo-bleached (Fig. 2C). CFP images that were acquired before (pre) and after photo-bleaching YFP (post) showed an increase in the intensity of CFP emission in Asef2-expressing cells (Fig. 2C), indicating FRET had occurred. Quantification revealed that Asef2 did indeed increase the FRET efficiency of the Raichu-Rac probe (Fig. 2C), showing that Asef2 significantly enhances the level of active Rac in cells.

To determine whether Asef2 inhibition of migration on type I collagen was dependent on Asef2 GEF activity, we generated a GEF deficient mutant. We mutated lysine 382 within the DH domain of Asef2 to alanine (K382A). Mutation of this residue in the related GEF collybistin impaired its GEF activity (Reddy-Alla et al., 2010). In an active Rac pulldown assay, GFP–Asef2 expression significantly enhanced the level of active Rac in HT1080 cells compared to GFP control cells (Fig. 2D). In contrast, expression of the Asef2 GEF mutant (GFP–Asef2-K382A) did not increase the amount of active Rac (Fig. 2D), indicating that the K382A mutation abolished GEF activity in Asef2. The migration speed of cells expressing GFP–Asef2-K382A was comparable to that observed in cells expressing GFP, whereas expression of GFP–Asef2 led to a significant decrease in migration speed (Fig. 2E). Thus, the GEF activity of Asef2 is crucial for the function of Asef2 in impairing migration on type I collagen.

Asef2 promotes larger adhesions that turn over slowly on type I collagen

Because adhesion assembly and disassembly (adhesion turnover) at the leading edge of cells is an important process that underlies migration, we hypothesized that the slower migration promoted by Asef2 resulted from impaired adhesion turnover. We began to test this hypothesis by immunostaining GFP and GFP–Asef2 stably expressing HT1080 cells for paxillin, a well-known adhesion marker. In GFP–Asef2 cells, the adhesions appeared larger than those observed in GFP cells, suggesting that adhesion

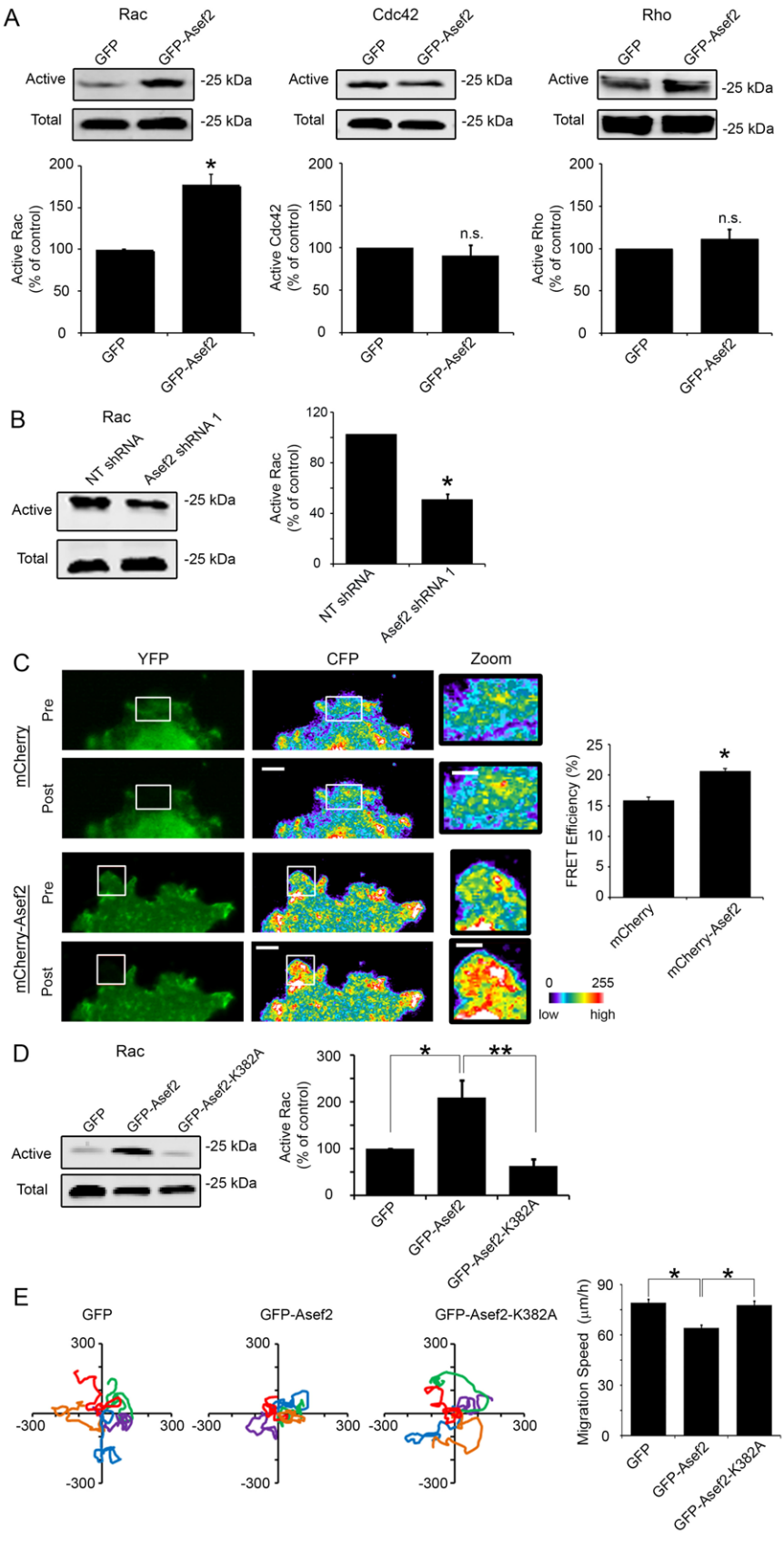

Fig. 2. Asef2 enhances activation of Rac and regulates migration through its GEF activity. (A) Upper, the active forms of Rac, Cdc42 and Rho were pulled down from lysates of GFP and GFP–Asef2 cells plated on type I collagen. The total level of these GTPases is shown as a control. Lower, quantification of the amount of active Rac, Cdc42, and Rho from at least three separate experiments. Error bars represent the s.e.m. *P<0.006, n.s. denotes no statistically significant difference. (B) Left, wild-type HT1080 cells were transfected with NT shRNA or Asef2 shRNA 1, and 3 days later, active Rac was pulled down from lysates. The total level of Rac is shown as a control. Right, quantification of the amount of active Rac from three independent experiments. Error bars represent the s.e.m. *P<0.0002. (C) HT1080 cells co-expressing the Raichu-Rac FRET probe and either mCherry or mCherry–Asef2 were subjected to acceptor photo-bleaching FRET analysis. Left, images of YFP and CFP before (Pre) and after (Post) photo-bleaching YFP with a 514 nm laser. The white square boxes denote the ROI where YFP was bleached. High-magnification images of the CFP intensity in the bleached ROIs (Zoom). CFP intensities are depicted on a pseudo-color scale in which lower intensity values are displayed in cool colors, whereas higher intensity values are displayed in warm colors. Scale bars: 5 μm (CFP panels), 2 μm ('Zoom' panels). Right, quantification of the average FRET efficiency of the Raichu-Rac FRET probe in mCherry and mCherry–Asef2 expressing cells. Error bars represent s.e.m. for 93–107 cells from three separate experiments. *P<0.0001. (D) Left, the active form of Rac was pulled down from lysates of wild-type HT1080 cells that were co-transfected with FLAG–Rac and either GFP, GFP–Asef2, or GFP–Asef2 in which lysine 382 in the DH domain was mutated to alanine (GFP–Asef2-K382A). Right, quantification of the amount of active Rac from blots from four independent experiments. Error bars represent the s.e.m. *P<0.03, **P<0.01. (E) HT1080 cells were transfected with GFP, GFP–Asef2 or GFP–Asef2-K382A and used in migration assays. Left, Rose plots of migration tracks of transfected cells. Right, quantification of the migration speed of cells transfected with GFP, GFP–Asef2 or GFP–Asef2-K382A. Error bars represent the s.e.m. for at least 70 cells from six independent experiments. *P<0.0001.

turnover was slower in these cells (Fig. 3A). Indeed, when adhesion turnover was quantified using an assay that we previously developed (Webb et al., 2004), the $t_{1/2}$ values for adhesion assembly and disassembly were increased by ~2-fold and 1.5-fold, respectively, in GFP–Asef2 cells compared with GFP control cells (Fig. 3B). These results indicate that adhesions are assembling and disassembling significantly more slowly in GFP–Asef2 cells.

Because binding of active (high-affinity state) integrins to the ECM initiates the assembly of adhesions (Hynes, 1992; Welf et al., 2012), Asef2 could affect adhesion turnover by altering the amount of active integrins at the cell membrane. To examine cell surface levels of active β1 integrin, a major integrin that binds to type I collagen, GFP and GFP–Asef2 cells were incubated with HUTS-4 antibody and subjected to flow cytometry. HUTS-4 antibody specifically binds to the activated conformation of β1 integrin (Luque et al., 1996). The amount of cell-surface active β1 integrin was increased ~3-fold in GFP–Asef2 cells compared with GFP controls, whereas the total level of β1 integrin was not significantly different (Fig. 3C). Moreover, as determined by total internal reflection microscopy (TIRF), the level of active β1 integrin in adhesions was significantly higher in GFP–Asef2 cells than in GFP cells, whereas the amount of total β1 integrin was comparable in these cells (Fig. 3D). Interestingly, the Asef2-promoted increase in the level of active β1 integrin in adhesions was diminished by treatment of GFP–Asef2 cells with the Rac specific inhibitor NSC23766 (supplementary material Fig. S3B). NSC23766 specifically blocks Rac binding and activation by its GEFs (Gao et al., 2004). Furthermore, the amount of active β1 integrin in adhesions was increased in GFP–Asef2 stably expressing MDA-MB-231 cells compared to GFP control cells (supplementary material Fig. S2B). In addition, knockdown of endogenous Asef2 in HT1080 cells with Asef2 shRNA 1 decreased the level of active β1 integrin in adhesions compared to cells transfected with NT shRNA (Fig. 3E). Thus, our data suggest that activation of Rac by Asef2 slows the turnover of adhesions by increasing the level of active β1 integrin in these structures.

Traction force and cell contractility are enhanced by Asef2

Because a major role for adhesions is to transmit traction forces to the ECM (Balaban et al., 2001; Beningo et al., 2001), we hypothesized that Asef2 functions by increasing the traction force in cells. Using traction force microscopy, we created vector maps of the traction stresses (force per unit area) that were generated by GFP and GFP–Asef2 stably expressing HT1080 cells. The vector maps showed that the traction stresses were significantly higher in GFP–Asef2 cells compared to GFP controls (Fig. 4A). Relatively high traction stresses were observed throughout GFP–Asef2 cells, but the largest stresses were seen at the cell edge. Quantification revealed that the average traction stress was ~4-fold greater in GFP–Asef2 cells compared with GFP cells. These results demonstrate that Asef2 dramatically enhances traction stresses in cells.

Previous work has shown that actomyosin contractility promotes the maturation of adhesions (Choi et al., 2008; Chrzanowska-Wodnicka and Burridge, 1996). Given that Asef2 induces larger adhesions as well as slowing adhesion turnover, it could function in regulating contractility. To examine the effect of Asef2 on contractility, we used a gel contraction assay (Tovell et al., 2011; Vernon and Gooden, 2002). In this assay, GFP and GFP–Asef2 cells were incubated in type I collagen gels for 14 hours to allow for contraction of the gels by cells. Contractility was assessed by measuring the diameter of gels at the beginning and at the end of the incubation period. At the end of the assay, the diameters of gels that contained GFP–Asef2 cells were significantly reduced compared to those containing GFP cells (Fig. 4B), indicating greater gel contraction by Asef2 cells. When contraction was quantified by expressing the gel diameters at the end of the assay (contracted gels) as a percentage of the original gel diameters, gels containing GFP–Asef2 stable HT1080 cells were decreased by ~40% compared to those containing GFP cells (Fig. 4B). Similar results were observed with GFP–Asef2 stably expressing MDA-MB-231 cells (supplementary material Fig. S2C). In addition, knockdown of endogenous Asef2 in HT1080 cells led to an increase in gel diameters compared to those observed with NT shRNA transfected cells, indicating that Asef2 knockdown reduced gel contraction (Fig. 4C). Taken together, these results demonstrate that Asef2 increases contractility in cells.

Asef2 regulates migration by increasing MyoII activity

As our results show that Asef2 increases contractility, and MyoII activity is known to modulate contractility in cells (Adelstein and Conti, 1975; Scholey et al., 1980), we next examined the role of MyoII in mediating Asef2 function. MyoII activity is regulated by phosphorylation of S19 in its RLCs, and thus, the phosphorylation state of this residue can be used to assess MyoII activity (Ikebe, 1989; Matsumura et al., 1998). We determined the level of active MyoII in GFP and GFP–Asef2 stably expressing HT1080 cells by immunostaining with antibody against MyoII phosphorylated at S19 (phospho-S19 MyoII) and imaging with fluorescence microscopy. As shown in Fig. 5A, the amount of phospho-S19 MyoII (p-S19 MyoII; active MyoII) was greater in GFP–Asef2 stably expressing HT1080 cells than in GFP cells. When the fluorescence intensity of active MyoII was quantified for individual cells, the amount of active MyoII was increased ~1.5-fold in GFP–Asef2 cells compared to that observed in GFP cells, whereas the level of total MyoII was not significantly different in these cells (Fig. 5A). Moreover, the amount of active MyoII was increased in GFP–Asef2 stable MDA-MB-231 cells compared with GFP controls (supplementary material Fig. S2D). Conversely, knockdown of endogenous Asef2 in HT1080 cells led to a decrease in the level of active MyoII (Fig. 5B). Thus, these results indicate that Asef2 increases the level of active MyoII in cells.

To further demonstrate that Asef2 modulates MyoII activity in cells, we performed In-Cell western assays. In this assay, GFP and GFP–Asef2 stably expressing HT1080 cells were allowed to adhere to 96-well culture plates coated with type I collagen and subsequently immunostained for phospho-S19 MyoII or total MyoII followed by fluorescently-conjugated secondary antibody. The background-subtracted integrated fluorescence intensity in each well was then quantified. The amount of active MyoII was ~1.7-fold higher in GFP–Asef2 cells compared to GFP controls, whereas the level of total MyoII was not significantly different in these cells (Fig. 5C). Collectively, these results show that Asef2 significantly enhances the amount of active MyoII in cells plated on type I collagen and point to Asef2 as an important regulator of MyoII activity.

Our data also raised the question as to whether Asef2 regulates cell migration on type I collagen through its ability to modulate

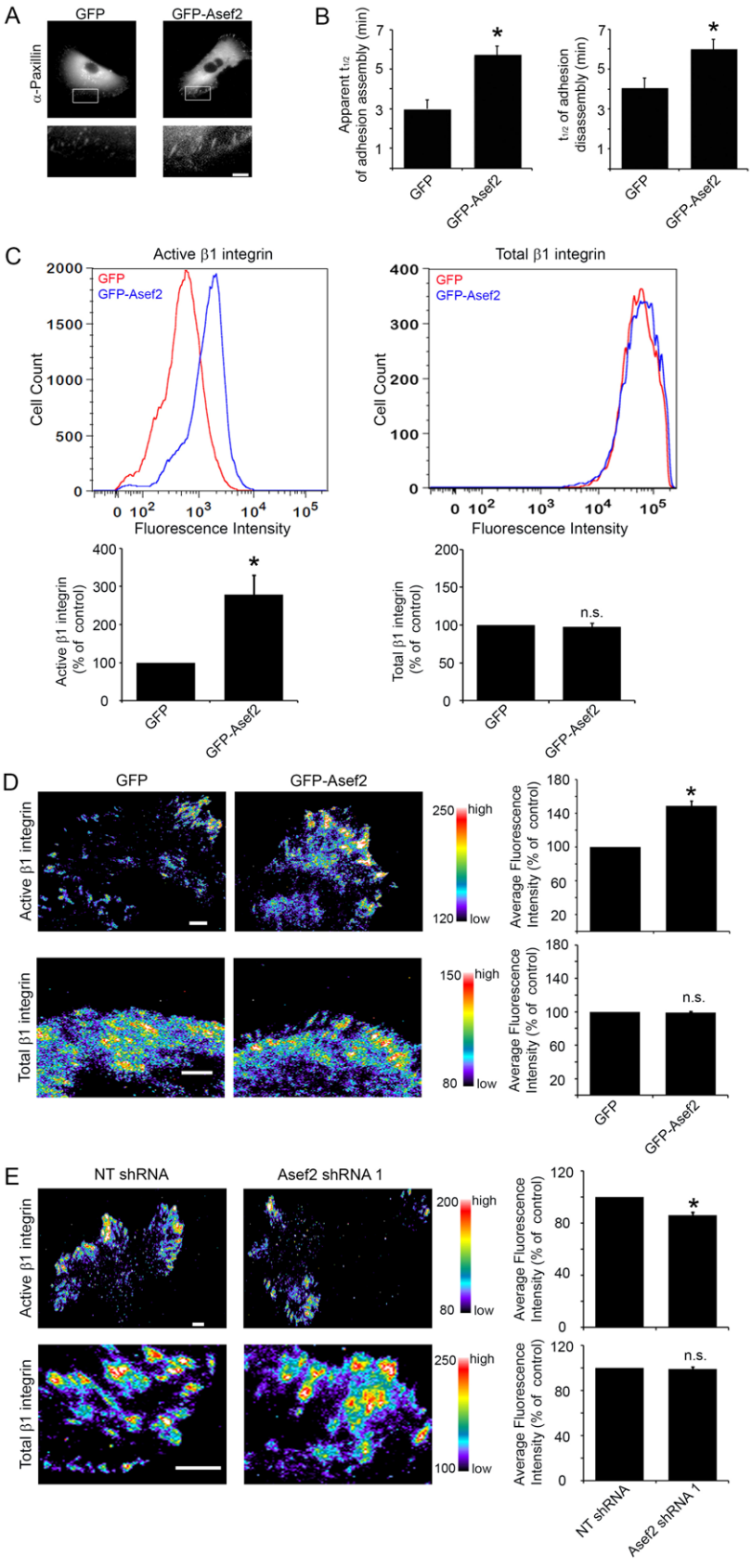

Fig. 3. Asef2 increases the amount of active β1 integrin in adhesions and slows adhesion turnover. (A) Upper, GFP and GFP–Asef2 cells were immunostained for paxillin, a well-characterized adhesion marker. Lower, higher magnification images of the boxed regions in the upper panels. Scale bar: 5 µm. (B) GFP and GFP–Asef2 cells were transfected with mCherry–paxillin and used in adhesion turnover assays. Quantification of the apparent $t_{1/2}$ for adhesion assembly and the $t_{1/2}$ for adhesion disassembly. Error bars represent the s.e.m. for 20–25 adhesions from four or five cells from three separate experiments. *P<0.0001. (C) Left, GFP and GFP–Asef2 cells were incubated with HUTS-4 antibody, which recognizes active β1 integrin, and fluorescently conjugated secondary antibody. HUTS-4 antibody binding to active β1 integrin on cells was measured using flow cytometry, and histograms are shown. Right, the total level of β1 integrin on GFP and GFP–Asef2 cells were assessed using AIIB2 antibody and flow cytometry. Histograms are shown. Lower, quantification of HUTS-4 (active β1 integrin) and AIIB2 (total β1 integrin) binding to GFP and GFP–Asef2 cells. Error bars represent s.e.m. from three separate experiments. *P<0.0001. (D) Left, GFP and GFP–Asef2 cells were immunostained for active or total β1 integrin and subjected to TIRF microscopy. Scale bar: 5 µm. Right, quantification of the amount of active β1 integrin (upper panel) and total β1 integrin (lower panel) in adhesions from GFP and GFP–Asef2 cells. Error bars represent s.e.m. from at least 60 adhesions from three separate experiments. *P<0.002. (E) Left, wild-type HT1080 cells were transfected with NT shRNA or Asef2 shRNA 1. After 3 days, cells were immunostained for active or total β1 integrin and subjected to TIRF microscopy. Scale bar: 5 µm. Right, quantification of the amount of active and total β1 integrin in adhesions from NT shRNA and Asef2 shRNA 1 transfected cells. Error bars represent s.e.m. from at least 59 adhesions from three separate experiments. *P<0.0003. For panels D and E, active and total β1 integrin images are shown in pseudo-color coding. For panels C–E, n.s. denotes no statistically significant difference.

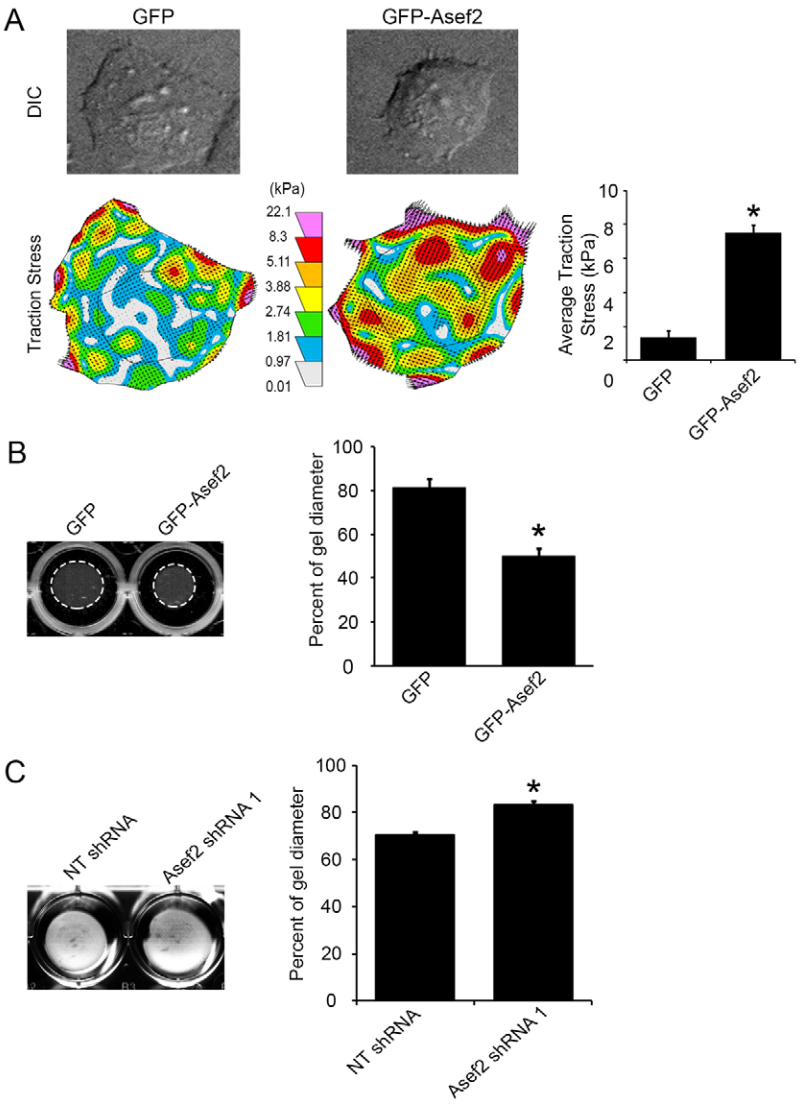

Fig. 4. Traction force and cell contractility are significantly increased by Asef2. (A) GFP and GFP–Asef2 stably expressing HT1080 cells were cultured in polyacrylamide (PAA) gels, embedded with FluoSpheres® fluorescent beads, for traction stress measurements. Upper, DIC images of GFP and GFP–Asef2 cells in PAA gels. Lower, color-coded vector maps show traction stresses produced by these cells. In the vector maps, the length and orientation of arrows indicate the magnitude and direction of traction stresses. Right, quantification of average traction stresses generated by GFP and GFP–Asef2 cells. Error bars represent the s.e.m. for 25 cells from at least three individual experiments. *$P<0.003$. (B) GFP and GFP–Asef2 stable HT1080 cells were embedded in type I collagen gels, and gels were incubated for 14 hours at 37℃ to allow for contraction. Left, images of contracted gels with GFP and GFP–Asef2 cells. The gel circumferences are outlined with dotted white lines. Right, at the end of the contraction assay, the diameter of the gels was measured and expressed as a percentage of the original gel diameter (before contraction). Error bars represent s.e.m. from three independent experiments. *$P<0.0002$. (C) Wild-type HT1080 cells were transfected with NT shRNA or Asef2 shRNA 1 and used in type I collagen gel contraction assays 3 days later. Left, images of contracted gels with NT shRNA and Asef2 shRNA 1 transfected cells. Right, quantification of gel contraction for cells transfected NT shRNA or Asef2 shRNA 1. Error bars represent s.e.m. from three independent experiments. *$P<0.0005$.

MyoII activity. To address this question, we inhibited MyoII with blebbistatin, which impairs the ATPase activity of MyoII (Kovács et al., 2004; Straight et al., 2003), and assessed migration. Treatment of GFP control cells with blebbistatin led to an increase in migration speed (Fig. 6A,B), which is consistent with previous studies (Even-Ram et al., 2007; Liu et al., 2010; Niggli et al., 2006). At the end of the migration assay, we performed washout experiments to show that the effects on migration were due to blebbistatin. In these experiments, blebbistatin-containing medium was removed, cells were washed, fresh medium without blebbistatin was added, and cells were used in migration assays. The migration speed of GFP cells after washout was decreased compared to that observed in GFP cells treated with blebbistatin (Fig. 6A,B). Indeed, the migration speed of GFP cells following washout was similar to that seen in vehicle-treated control cells (Fig. 6A,B). Consistent with our previous results, the migration speed of GFP–Asef2 cells was decreased when compared to GFP cells. Treatment of GFP–Asef2 cells with blebbistatin resulted in a significant increase in migration speed, and blebbistatin washout negated the increase in migration (Fig. 6A,B), indicating that MyoII activity is crucial for the effect of Asef2 on migration. Collectively, our data suggest that Asef2 regulates migration by modulating MyoII activity and function.

We had previously shown that Asef2 regulates cell migration on fibronectin by a mechanism that is dependent on Rac and the serine/threonine kinase Akt (Bristow et al., 2009). Here, we demonstrate that Asef2 modulates migration on type I collagen by increasing Rac and MyoII activity. This raises the question as to whether Akt also contributes to the regulation of Asef2-mediated migration on type I collagen. To address this question, we plated GFP and GFP–Asef2 stably expressing HT1080 cells on type I collagen and immunostained with antibody against Akt phosphorylated on threonine 308 (phospho-T308 Akt). T308 is one of the key residues that is phosphorylated when Akt is activated; therefore, phospho-T308 Akt antibody can be utilized to detect active Akt (Alessi et al., 1996). Interestingly, the amount of active Akt was similar in GFP and GFP–Asef2 cells plated on type I collagen (supplementary material Fig. S1C), suggesting that the Asef2-Rac signaling mechanisms are different for cells plated on fibronectin and type I collagen. To further investigate Asef2-Rac signaling on these substrates, we plated

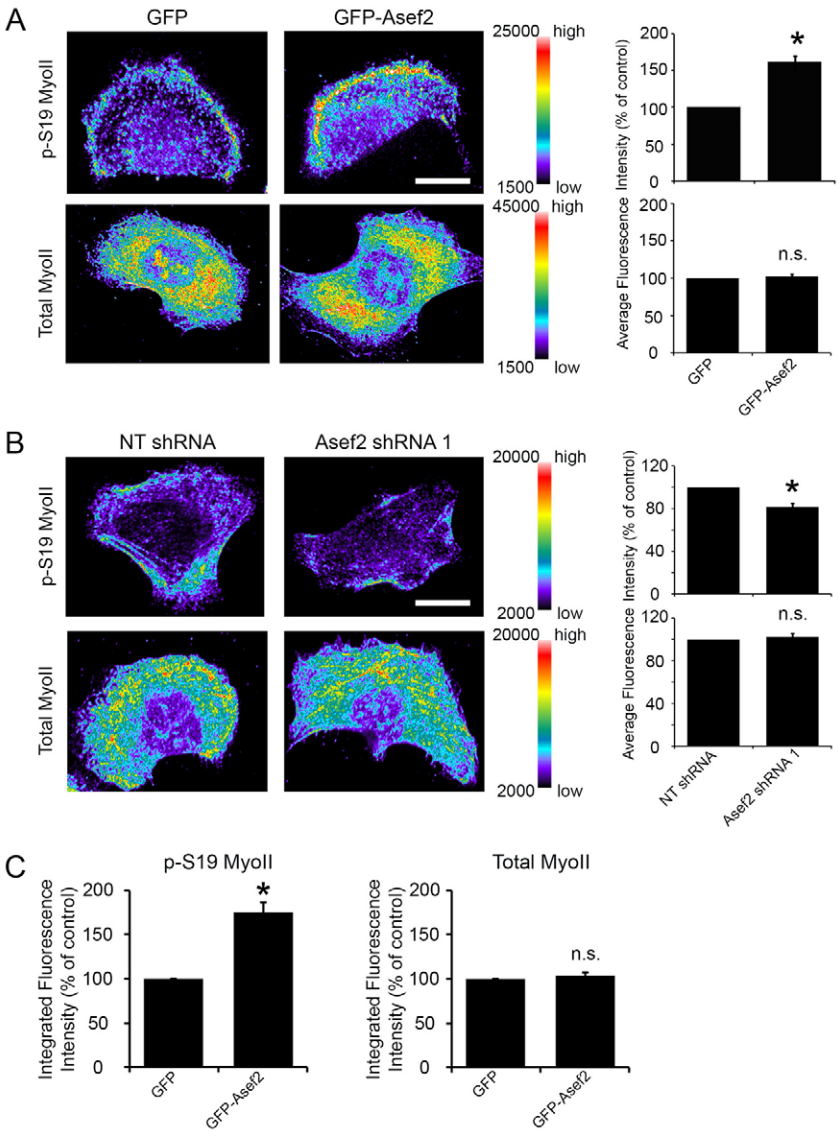

Fig. 5. Asef2 increases phosphorylation of MyoII at S19. (A) Left, GFP and GFP–Asef2 stably expressing HT1080 cells were immunostained for MyoII phosphorylated at S19 (p-S19 MyoII) or total MyoII. Scale bar: 15 µm. Right, quantification of the amount of p-S19 Myo II (upper panel) and total MyoII (lower panel) in GFP and GFP-Asef2 cells. Error bars represent the s.e.m. for at least 117 cells from at least six individual experiments. *$P<0.002$. (B) Left, wild-type HT1080 cells were transfected with NT shRNA or Asef2 shRNA 1. After 3 days, cells were immunostained for S19 phosphorylated MyoII (p-S19 MyoII) or total MyoII. Scale bar: 15 µm. Right, quantification of the amount of p-S19 MyoII and total MyoII in NT shRNA and Asef2 shRNA 1 transfected cells. Error bars represent the s.e.m. for at least 58 cells from at least four individual experiments. *$P<0.004$. (C) GFP and GFP–Asef2 cells were subjected to In-Cell western analysis using antibodies against S19 phosphorylated MyoII (p-S19 MyoII) or total MyoII. Left, quantification of the amount of p-S19 MyoII in GFP and GFP-Asef2 cells. Error bars represent s.e.m. from four separate experiments. *$P<0.001$. Right, quantification of the amount of total MyoII in GFP and GFP–Asef2 cells. Error bars represent the s.e.m. from four separate experiments. n.s. denotes no statistically significant difference.

GFP and GFP–Asef2 stably expressing HT1080 cells on fibronectin and immunostained for active MyoII with phospho-S19 MyoII antibody. The amount of active MyoII was not significantly different in GFP and GFP–Asef2 cells plated on fibronectin (supplementary material Fig. S1D). Therefore, our results suggest that Asef2-Rac signaling regulates migration on fibronectin and type I collagen by distinct molecular mechanisms.

Activation of Rac by Asef2 regulates MyoII contractility

Because Asef2 increased the amount of active Rac and modulated MyoII activity, we hypothesized that Rac regulates MyoII contractility. To begin to test this hypothesis, we used two shRNA constructs to knockdown endogenous expression of Rac and then assessed MyoII activity by immunostaining with phospho-S19 MyoII antibody. These shRNAs have been previously shown to knockdown endogenous Rac expression in HT1080 cells by ~75% (Bristow et al., 2009). Transfection of GFP stably expressing HT1080 cells with the Rac shRNAs led to an ~2-fold reduction in the amount of active MyoII compared with that observed in cells transfected with pSUPER or NT shRNA (Fig. 7A), indicating that inhibition of basal Rac expression significantly decreased the level of active MyoII. In GFP–Asef2 stably expressing HT1080 cells, the level of active MyoII was significantly increased compared with control cells, and expression of the Rac shRNAs dramatically reduced the amount of active MyoII in these cells (Fig. 7A). Indeed, the level of active MyoII in GFP–Asef2 cells transfected with the Rac shRNAs was similar to that observed in GFP cells transfected with these knockdown constructs (Fig. 7A), indicating that Rac knockdown abrogated the Asef2-mediated effect on MyoII activity. Similar results were obtained when GFP and GFP–Asef2 cells were treated with the Rac inhibitor NSC23766 (supplementary material Fig. S3A). Neither the Rac shRNAs nor NSC23766 affected the level of total MyoII in cells (Fig. 7A; supplementary material Fig. S3A). Taken together, these results suggest that Rac activity regulates the amount of active MyoII in cells, and Asef2 regulates MyoII through Rac.

Next, we examined the effect of Rac activity on Asef2-mediated contractility by using GFP and GFP–Asef2 cells that

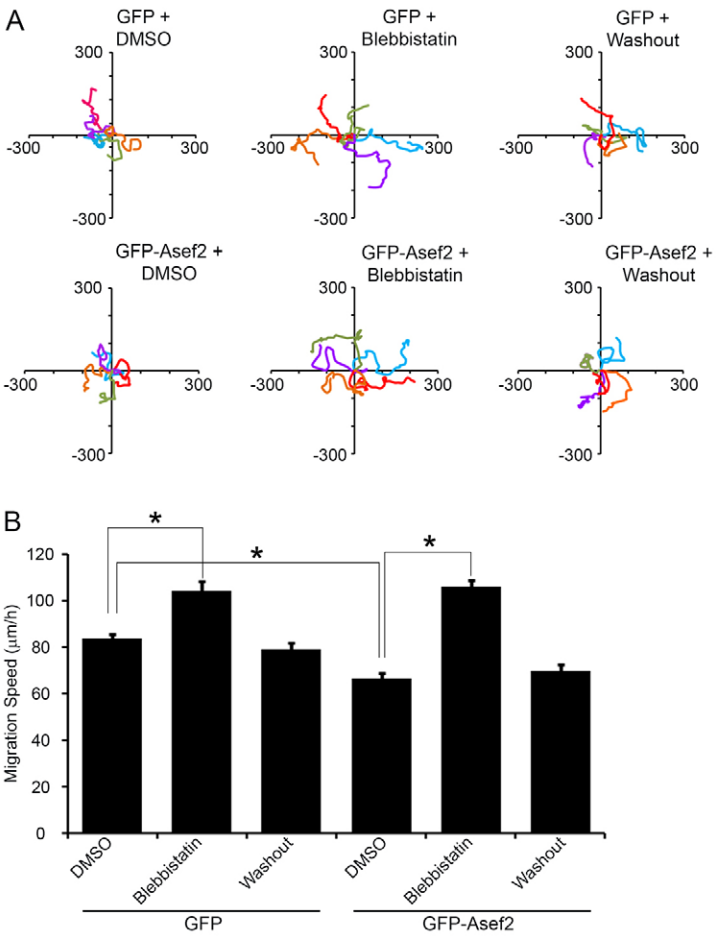

Fig. 6. Inhibition of MyoII with blebbistatin enhances basal migration and abolishes the Asef2-mediated decrease in migration on type I collagen. (A) GFP and GFP–Asef2 stably expressing HT1080 cells were pre-treated with 20 μM blebbistatin or vehicle (DMSO) for 1 hour at 37℃ and then used in migration assays. After 6 hours, blebbistatin was replaced with fresh imaging medium (Washout), and cells were imaged for an additional 6 hours. Rose plots of the migration tracks for five cells for each treatment are shown. (B) Quantification of the migration speed for GFP and GFP–Asef2 cells with the indicated treatments. Error bars represent s.e.m. for at least 30 cells from three independent experiments. *$P<0.0001$.

were treated with NSC23766 in gel contraction assays. In GFP–Asef2 cells, the gel diameters were significantly reduced compared to those observed in GFP cells (Fig. 7B), demonstrating that Asef2 enhances contractility. Treatment of GFP–Asef2 cells with NSC23766 diminished the increased contractility (Fig. 7B), suggesting that Rac activity induced by Asef2 promotes the enhanced contractility observed with these cells. To further show that Rac modulated contractility, we knocked down Rac in GFP–Asef2 cells using the two Rac shRNAs. Consistent with our previous results, GFP–Asef2 cells transfected with empty pSUPER vector or a NT shRNA showed enhanced contractility, with their gel diameters contracted to less than half of their original diameters (Fig. 7C). Transfection of GFP–Asef2 cells with the Rac shRNAs led to significantly less gel contraction compared to that seen with cells transfected with pSUPER or NT shRNA (Fig. 7C). Collectively, our results show that Asef2 increases gel contraction through Rac, thus, highlighting an important new role for Rac in regulating contractility within cells.

Discussion

Actomyosin contractility plays a crucial role in regulating cell migration through its ability to modulate underlying processes (Clark et al., 2007). Rho is a well-characterized regulator of actomyosin contractility (Wheeler and Ridley, 2004), but the function of other GTPases, such as Rac, in controlling this process is currently poorly understood. Here, we demonstrate that activation of Rac by Asef2 increases MyoII contractility to inhibit cell migration. Knockdown of endogenous Rac using shRNAs or inhibition of Rac activation resulted in a significant decrease in MyoII activity as determined by immunostaining for phosphorylated S19 on MyoII RLCs. In addition, Rac knockdown or inhibition led to a decrease in cell contractility. In contrast, an increase in Rac activity by Asef2 induced MyoII S19 phosphorylation and significantly enhanced cell contractility. Thus, we demonstrate a new function for Rac in regulating actomyosin contractility, which is important for cell migration.

Rac is likely to modulate actomyosin contractility through downstream effectors. One possibility is PAK, which has been shown to phosphorylate RLCs of MyoII on S19 (Chew et al., 1998; Kiosses et al., 1999; Zeng et al., 2000). Moreover, expression of constitutively active Rac led to an increase in S19 phosphorylation of MyoII RLCs, which was mediated, at least in part, through PAK (Brzeska et al., 2004). However, other studies have shown that PAK phosphorylates and inhibits myosin light chain kinase (MLCK), which activates MyoII through phosphorylation of S19 (Goeckeler et al., 2000; Sanders et al., 1999; Wirth et al., 2003). In this case, activation of PAK would decrease MyoII contractility through inhibition of MLCK. Clearly, the effects of PAK on contractility are complex and probably involve the interplay between PAK and other regulators. Therefore, it is entirely possible that other Rac effectors are involved in mediating Rac-induced MyoII-dependent contractility. Identifying the specific Rac effectors that modulate contractility represents an exciting avenue for future studies.

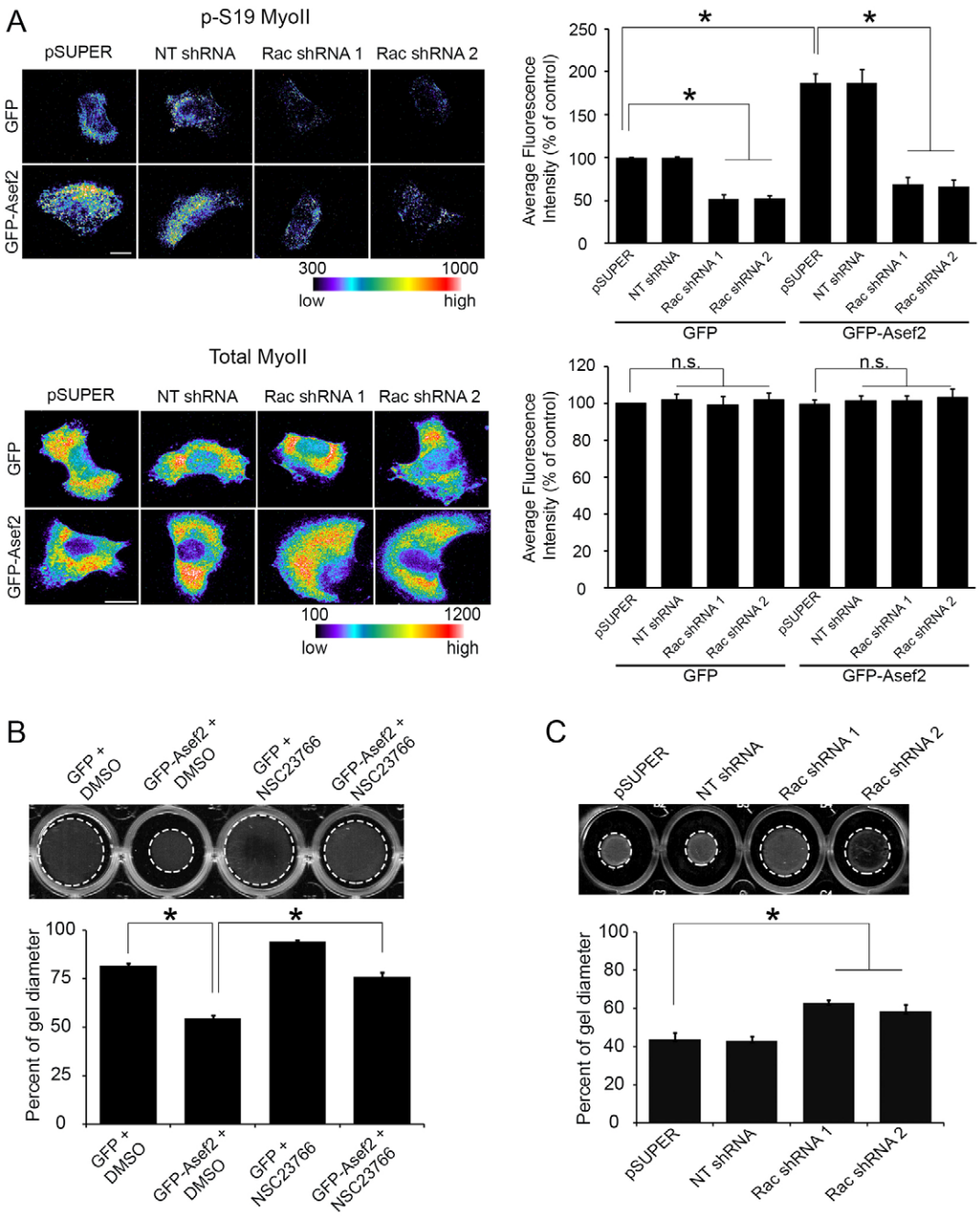

Fig. 7. Activation of Rac by Asef2 stimulates MyoII-dependent contractility. (A) Left, GFP and GFP–Asef2 stably expressing HT1080 cells were co-transfected with mCherry and either empty pSUPER vector, a NT shRNA or Rac shRNAs. After 3 days, cells were immunostained with antibodies that recognize S19 phosphorylated MyoII (p-S19 MyoII; upper panels) or total MyoII (lower panels). Scale bar: 15 μm. Right, quantification of the level of p-S19 Myo II (upper panel) and total MyoII (lower panel) in GFP and GFP–Asef2 cells. Error bars represent s.e.m. for 30 cells from three individual experiments. *$P<0.002$. n.s. denotes no statistically significant difference. (B) GFP and GFP–Asef2 stably expressing HT1080 cells were incubated with the Rac inhibitor NSC23766 or DMSO and then used in type I collagen gel contraction assays. Upper, images of contracted gels from GFP and GFP–Asef2 cells treated with DMSO or NSC23766. Lower, quantification of gel contraction for GFP and GFP–Asef2 cells with the indicated treatments. Error bars represent the s.e.m. from three individual experiments. *$P<0.0001$. (C) GFP–Asef2 stably expressing HT1080 cells were co-transfected with mCherry and empty pSUPER vector, a NT shRNA, or Rac shRNAs and were used in type I collagen gel contraction assays 3 days later. Upper, images of contracted gels from cells transfected with the indicated constructs. Lower, quantification of gel contraction for cells transfected with the indicated constructs. Error bars represent s.e.m. from three individual experiments. *$P<0.004$. For panels B and C, the gel circumferences are outlined with dotted white lines.

A known function of MyoII contractility is to promote the maturation of adhesions (Choi et al., 2008; Chrzanowska-Wodnicka and Burridge, 1996). Our results show that Asef2 generates large adhesions that turn over slowly in protrusive regions of cells. Asef2 activation of Rac increases actomyosin contractility, which could serve to induce the maturation of

adhesions. As a result, the nascent adhesions that form at the leading edge do not disassemble, but instead continue to grow into large focal adhesions. These large, mature adhesions can impair cell migration given that adhesion turnover at the leading edge is essential for driving rapid migration (Laukaitis et al., 2001; Webb et al., 2004).

In this study, we show that Asef2 activation of Rac inhibits cell migration, when cells are plated on type I collagen, through regulation of actomyosin contractility. We previously demonstrated that Asef2 promotes migration on fibronectin through activation of Rac and the serine/threonine kinase Akt, which subsequently leads to a decrease in Rho activity (Bristow et al., 2009). Interestingly, in both cases, Asef2 modulates cell migration by increasing Rac activity; however, the effects on migration and contractility are quite different. Although the factors that contribute to these differences are currently unknown, it is tempting to speculate that scaffolding proteins are involved. Scaffolding proteins can recruit or bring together various binding partners, through their multiple protein–protein interaction domains, and dictate signaling to various downstream targets (Pawson, 2007). Through the recruitment of Asef2, Rac and particular downstream effectors, scaffolding proteins could provide a mechanism for specificity in Rac signaling. Another Rac GEF, Tiam1, has been shown to associate with different scaffolding proteins to selectively activate distinct downstream Rac effectors (Buchsbaum et al., 2002; Buchsbaum et al., 2003). Scaffolding proteins could also contribute to the selectivity of the GTPases by recruiting Asef2 and Rac to the complex to enhance Asef2 activation of Rac over other GTPases, such as Cdc42. Interestingly, our results show that Asef2 activates Rac, but not Cdc42, when cells are plated on type I collagen. The interaction of Asef2 and distinct scaffolding proteins could provide a mechanism by which this GEF could selectively activate one GTPase instead of another.

In summary, our study has uncovered an unconventional mechanism by which Rac regulates cell migration. Activation of Rac by Asef2 enhances MyoII contractility, which had been classically thought to be mediated by Rho. Asef2, through Rac, promotes the phosphorylation of S19 in the RLCs of MyoII to increase actomyosin contractility. The increased actomyosin contractility, in turn, might affect underlying migratory processes, such as adhesion dynamics, to modulate cell migration.

Materials and Methods

Reagents

An anti-Asef2 rabbit polyclonal antibody was made as previously described (Bristow et al., 2009). β1 integrin HUTS-4 monoclonal antibody was purchased from Chemicon International (Temecula, CA). AIIB2 β1 integrin antibody was kindly provided by Roy Zent (Vanderbilt University, Nashville, TN). Phospho-MLC (S19) polyclonal antibody (clone 3671) was obtained from Cell Signaling (Beverly, MA). Phospho-Akt (T308) polyclonal antibody was purchased from Santa Cruz Biotechnology (Santa Cruz, CA). Fibronectin, β-actin monoclonal antibody (clone AC-15) and FLAG-M2 monoclonal antibody were from Sigma-Aldrich (St. Louis, MO). Paxillin monoclonal antibody was purchased from BD Bioscience Pharmingen (San Diego, CA). Alexa-Fluor-555- and Alexa-Fluor-680-conjugated anti-mouse Ig, Alexa-Fluor-647-conjugated anti-rabbit Ig, and FluoSpheres® carboxylate-modified Nile Red microspheres (Cat. No. F-8819) were obtained from Molecular Probes (Eugene, OR). IRDye 800 anti-mouse Ig and 800 anti-rabbit Ig were purchased from Rockland Immunochemicals (Gilbertsville, PA). Rat tail type I collagen was from BD Biosciences (Bedford, MA). Blebbistatin, NSC23766 and BSA were purchased from EMD Bioscience (La Jolla, CA). Aqua Poly/Mount mounting solution (Cat # 18606) was obtained from Polysciences, Inc. (Warrington, PA).

Plasmids

GFP–Asef2-encoding cDNA was prepared by cloning full-length Asef2 (*Spata13*) cDNA into pEGFP-C3 vector as previously described (Bristow et al., 2009). mCherry cDNA was a generous gift from Roger Tsien (University of California, San Diego, La Jolla, CA). mCherry–paxillin was kindly provided by Steve Hanks (Vanderbilt University, Nashville, TN). GST-tagged PBD, wild-type Cdc42 and wild-type Rac1 were kind gifts from Alan Hall (Memorial Sloan-Kettering Cancer Center, NY). GST-tagged rhotekin-binding domain and Myc-tagged wild-type RhoA were generously provided by Sarita Sastry (University of Texas Medical Branch, Galveston,TX). shRNA constructs were generated as previously described (Wegner et al., 2008; Zhang and Macara, 2008) by ligating 64-mer oligonucleotides into GFP-pSUPER vector (Asef2 shRNAs) or pSUPER vector (Rac shRNAs). Both target sequences for Asef2 and Rac1 have been previously described (Bristow et al., 2009; Chan et al., 2005). A non-targeting shRNA with the sequence 5′-CAGTCGCGTTTGCGACTGG-3′ was used as a control (Saito et al., 2007).

Cell culture

HT1080 cells stably expressing GFP or GFP–Asef2 were generated by retroviral transduction and selected by incubation with 400 μg/ml G418 as previously described (Bristow et al., 2009). Stably expressing GFP and GFP–Asef2 cells were sorted by FACS into populations based on their expression level (Bristow et al., 2009). Experiments for this study were performed with stable cells expressing low levels of GFP or GFP–Asef2, which were the same cells that were used previously (Bristow et al., 2009). Cells were maintained in Dulbecco's modified Eagle's medium (DMEM) (Invitrogen, Carlsbad, CA) supplemented with 10% fetal bovine serum (FBS) (Hyclone, Logan, UT) and penicillin-streptomycin (Invitrogen). Wild-type HT1080 cells were transiently transfected with Lipofectamine™ 2000 (Invitrogen) according to the manufacturer's instructions. MDA-MB-231 cells stably expressing GFP or GFP–Asef2 were prepared by retroviral transduction as described above for HT1080 cells. Stably expressing GFP and GFP–Asef2 MDA-MB-231 cells were maintained in DMEM supplemented with 20% FBS and penicillin-streptomycin.

Microscopy and immunocytochemistry

Cells were plated on glass coverslips, which were coated with 5 μg/ml type I collagen or 2.5 μg/ml fibronectin for 1 hour at 37℃. Following incubation for 2–4 hours at 37℃ to permit attachment, cells were fixed for 20 minutes with 2–4% paraformaldehyde and 4% sucrose in phosphate-buffered saline (PBS). In some experiments, cells were fixed by incubation with ice-cold methanol for 10 minutes at −20℃. Cells were permeabilized for 5 minutes at 23℃ with 0.2% (v/v) Triton X-100, and incubated with either 20% goat serum or 10% BSA in PBS for 1 hour at 23℃ to block non-specific binding. After blocking, cells were incubated with the indicated primary and fluorescently conjugated secondary antibodies, which were diluted in either 5% goat serum or 2% BSA in PBS, for 1 hour at 23℃. Following each step, coverslips were washed three times with PBS. Coverslips were mounted on microscope glass slides (Fisher Scientific, Pittsburgh, PA) with Prolong Gold Antifade reagent (Invitrogen, Carlsbad, CA). Images were acquired with either an inverted Olympus IX71 microscope (Melville, NY) equipped with a Retiga EXi CCD camera (QImaging, Surrey, BC) and a PlanApo 60× OTIRFM objective (NA 1.45) or a Quorum WaveFX spinning disk confocal system with a Nikon Eclipse Ti microscope, a Hamamatsu ImageEM-CCD camera, and a PlanApo 60× TIRF objective (NA 1.49). To visualize GFP, an Endow GFP Bandpass filter cube (excitation HQ470/40, emission HQ525/50, Q495LP dichroic mirror) was used. Alexa Fluor® 555 and mCherry were observed using a TRITC/Cy3 cube (excitation HQ545/30, emission HQ610/75, Q570LP dichroic mirror), and Alexa Fluor® 647 (far-red) was observed with a Cy5™ cube (excitation HQ620/60, emission HQ700/75, Q660LP dichroic mirror). The background-subtracted integrated fluorescent intensity was normalized to cell area (average intensity).

For quantification of phosphorylated (S19) MyoII and total MyoII, the average fluorescence intensity was obtained by normalizing the background-subtracted integrated fluorescence intensity in individual cells to the unit area using MetaMorph software. For quantification of the amount of active and total β1 integrin in adhesions, the average fluorescence intensity was measured by normalizing the background-subtracted integrated fluorescence intensity in individual adhesions to the unit area with MetaMorph software.

In-cell western assay

At total of 10^4 cells were allowed to adhere for 2–4 hours at 37℃ to 96-well plates that were coated with 5 μg/ml type I collagen. After attachment, cells were incubated for 20 minutes at 23℃ with 4% paraformaldehyde in PBS and permeabilized for 5 minutes at 23℃ with 0.2% (v/v) Triton X-100. Cells were then incubated with 5% BSA in PBS (blocking solution) for 1 hour at 23℃ to block non-specific binding. Following blocking, cells were incubated with the indicated primary and fluorescently conjugated secondary antibodies in blocking solution for 1 hour at 23℃. Cells were washed three times with PBS after each incubation. After the final wash, 96-well plates were aspirated and inverted to remove the residual wash solution and scanned with a LI-COR® Odyssey® infrared imaging system (LI-COR Biosciences, Lincoln, NE). The background-subtracted mean integrated intensities were obtained using Odyssey® 3.2 ICW module software.

Background fluorescence was determined from cells that were incubated with secondary antibodies alone.

Migration assay

Cells were allowed to adhere for 1–2 hours at 37℃ to tissue culture dishes that were coated with 5 μg/ml type I collagen or 2.5 μg/ml fibronectin. Phase-contrast images were acquired every 5 minutes for up to 6 hours using MetaMorph software (Molecular Devices, Inc. Sunnyvale, CA), interfaced with a Lambda 10-2 automated controller (Sutter Instruments), and an Olympus IX71 microscope with a 10× objective (NA 0.3). During imaging, cells were maintained in SFM4MAb™ media (Hyclone, Logan, UT) supplemented with 2% FBS (imaging media). In some experiments, cells were pre-treated with 20 μM blebbistatin or DMSO (vehicle control) for 1 hour at 37℃. After pre-incubation, phase contrast images were acquired every 5 minutes for 6 hours. Then, blebbistatin was removed, cells were washed with PBS, fresh imaging medium was added, and cells were imaged for an additional 6 hours. MetaMorph software was used to track cell movement, and the migration speed was calculated by dividing the total distance that cells moved in microns by the time. Wind-Rose plots were obtained by setting the X-Y coordinates of cell tracks to a common origin.

Analysis of adhesion turnover

Stably expressing GFP and GFP–Asef2 cells were transfected with 1 μg of mCherry–paxillin-encoding cDNA. After 24 hours, cells were plated on microscopy dishes coated with type I collagen and allowed to adhere for 1–2 hours at 37℃. Time-lapse fluorescence images were acquired at 15-second intervals, and $t_{1/2}$ values for adhesion assembly and adhesion disassembly were calculated as previously described (Bristow et al., 2009; Webb et al., 2004).

Rho family GTPase activity assays

GFP and GFP–Asef2 stably expressing cells were transfected with 3 μg cDNA encoding FLAG–Rac1, FLAG–Cdc42 or Myc–RhoA. After 24 hours, cells were lysed and assayed for active Rac, Cdc42 and Rho as previously described (Bristow et al., 2009; Ren et al., 1999). In some experiments, wild-type HT1080 cells were co-transfected with 2 μg FLAG–Rac1 and 2 μg of either Asef2 shRNA 1 or NT shRNA. Three days later, lysates from cells were collected and analyzed as described above.

Traction force measurements

Polyacrylamide (PAA) gels embedded with 1.0 μm FluoSpheres® fluorescent beads were prepared on rectangular glass coverslips as previously described (Sabass et al., 2008). PAA gels were incubated with 140 μg/ml type I collagen for 4 hours at 23℃. The thickness of the PAA gels was ~30 μm, and the Young's modulus of the gels was 15.6 kPa as calculated previously (Sabass et al., 2008; Yeung et al., 2005). A total of 5×10^3 GFP or GFP–Asef2 stably expressing cells were incubated with PAA gels coated with type I collagen for 2 hours at 37℃ to allow cells to adhere. For each cell of interest, a DIC image of the cell and a fluorescence image of the FluoSpheres® beads with the attached cell were taken. Then, the cell of interest was dissociated from the PAA gel by trypsinization, and a fluorescence image of the FluoSpheres® beads was acquired. Images were acquired using the Quorum WaveFX spinning disk confocal system with a Nikon Eclipse Ti microscope, a Hamamatsu ImageEM-CCD camera, and a Plan Fluor 40× objective (NA 1.3). FluoSpheres® fluorescent beads were imaged using a 561 nm laser and a 593/40 nm BrightLine® single-band bandpass emission filter (Semrock, Rochester, NY). Traction force maps were generated from the acquired images using LIBTRC software (Dembo and Wang, 1999), which was developed by Micah Dembo (Boston University, Boston, MA).

FRET imaging and analysis

Wild-type HT1080 cells were co-transfected with the Raichu-Rac FRET probe (a kind gift from Michiyuki Matsuda, Kyoto University, Kyoto, Japan) and either mCherry–Asef2 or mCherry. After 24 hours, cells were plated on glass coverslips, which were coated with 5 μg/ml type I collagen, for 1 hour at 37℃. Cells were fixed by incubation for 15 minutes at 23℃ with a 4% paraformaldehyde (wt/vol) PBS solution containing 0.12 M sucrose. Coverslips were then mounted onto glass slides using Aqua Poly/Mount mounting solution. Images were acquired with a Zeiss LSM 510 Meta inverted confocal microscope using a Plan-Apochromat 63× objective (NA 1.4). CFP, YFP and mCherry fluorophores were excited with a 458, 514 and 543 nm laser, respectively. Images were collected using the following emission filters: CFP, BP 475–525 nm; YFP, LP 530 nm; and mCherry, LP 560 nm. mCherry images were used to identify cells expressing either mCherry–Asef2 or mCherry. CFP and YFP images were acquired both before and after bleaching YFP (the FRET acceptor) within an ROI. YFP images were taken to confirm that YFP was bleached within the ROI. CFP images were used to calculate the FRET efficiency of the active Rac FRET probe using the following equation: $(CFP_{Post}-CFP_{Pre})/CFP_{Post}\times100$. CFP_{Post} is the average intensity of CFP in the ROI after bleaching YFP with the 514 nm laser, and CFP_{Pre} is the average intensity of CFP in the ROI before bleaching YFP with the 514 nm laser. The average FRET efficiency of cells expressing mCherry-Asef2 was then compared to cells expressing mCherry using a Student's *t*-test statistical analysis.

Flow cytometry

GFP and GFP–Asef2 stably expressing cells were cultured on 5 μg/ml dishes coated with type I collagen for 18 hours at 37℃. Cells were then trypsinized (2.5% trypsin without EDTA) and resuspended in ice-cold Opti-MEM (GIBCO) containing 2% FBS (cell-sorting buffer). Cell suspensions (2.5×10^5 cells) were incubated with primary HUTS-4 antibody (1:500 dilution in cell-sorting buffer) for 30 minutes at 4℃ followed by secondary Alexa Fluor® 555 antibody (1:1000 dilution in cell-sorting buffer) for 20 minutes at 4℃. To determine non-specific binding, an equal amount of cell suspension was incubated with secondary antibody alone. Cells were washed three times with ice-cold cell-sorting buffer following each incubation. After the final wash, cells were resuspended in 500 μl of cell-sorting buffer and subjected to flow cytometry. For total β1 integrin staining, cells were incubated with AIIB2 antibody (1:50 dilution) and subjected to flow cytometry as described above. AIIB2 antibody binds to the extracellular domain of β1 integrin. Histograms were generated using FlowJo software.

Collagen gel contraction assay

Type I collagen gel contraction assays were performed as previously described (Tovell et al., 2011; Vernon and Gooden, 2002). Briefly, type I collagen was mixed with DMEM to a final concentration of 1.5 mg/ml and the pH was adjusted to 7.4 with 1 M NaOH. Cells in DMEM with 10% FBS were added to the type I collagen mixture to a final concentration of 2.5×10^5 cells per gel. This mixture was added to 24-well cell culture plates (Costar, Corning NY) and allowed to solidify by incubation for 1 hour at 37℃. Serum-free DMEM was added to the wells, and the collagen gels were gently detached using a pipette tip. The gels were incubated for 14 hours at 37℃, and then the diameter of the gels was measured. In some experiments, cells were incubated with 100 μM NSC23766 or DMSO as a vehicle control for 14 hours at 37℃.

Acknowledgements

We thank Alan Hall, Steve Hanks, Michiyuki Matsuda, Sarita Sastry, Roger Tsien and Roy Zent for providing us with reagents. We are grateful to Micah Dembo for providing us with an academic license to use the LIBTRC program. We thank Lan Hu and Mary Lynn Dear for assistance in preparing cDNA constructs and with the In-Cell western assay, respectively. FRET imaging was performed in part through the use of the VUMC Cell Imaging Shared Resource Core (supported by National Institutes of Health grants CA68485, DK20593, DK58404, HD15052, DK59637 and Ey008126).

Author contributions

L.J., D.M., and D.J.W. designed experiments. L.J. performed the majority of the experiments and data analysis. D.M., M.S., L.E.H., N.L.D., M.A., J.A.B., J.C.E., and D.P.C. performed experiments, analyzed data, and provided manuscript suggestions. L.J. and D.J.W. wrote the paper.

Funding

This work was supported by National Institutes of Health (NIH) [grant number GM092914 to D.J.W.]. J.A.B. was supported by a NIH pre-doctoral training grant [grant number CA078136]. Deposited in PMC for release after 12 months.

Supplementary material available online at
http://jcs.biologists.org/lookup/suppl/doi:10.1242/jcs.131060/-/DC1

References

Adelstein, R. S. and Conti, M. A. (1975). Phosphorylation of platelet myosin increases actin-activated myosin ATPase activity. *Nature* **256**, 597-598.

Alessi, D. R., Andjelkovic, M., Caudwell, B., Cron, P., Morrice, N., Cohen, P. and Hemmings, B. A. (1996). Mechanism of activation of protein kinase B by insulin and IGF-1. *EMBO J.* **15**, 6541-6551.

Balaban, N. Q., Schwarz, U. S., Riveline, D., Goichberg, P., Tzur, G., Sabanay, I., Mahalu, D., Safran, S., Bershadsky, A., Addadi, L. et al. (2001). Force and focal adhesion assembly: a close relationship studied using elastic micropatterned substrates. *Nat. Cell Biol.* **3**, 466-472.

Beningo, K. A., Dembo, M., Kaverina, I., Small, J. V. and Wang, Y. L. (2001). Nascent focal adhesions are responsible for the generation of strong propulsive forces in migrating fibroblasts. *J. Cell Biol.* **153**, 881-888.

Bristow, J. M., Sellers, M. H., Majumdar, D., Anderson, B., Hu, L. and Webb, D. J. (2009). The Rho-family GEF Asef2 activates Rac to modulate adhesion and actin dynamics and thereby regulate cell migration. *J. Cell Sci.* **122**, 4535-4546.

Brzeska, H., Szczepanowska, J., Matsumura, F. and Korn, E. D. (2004). Rac-induced increase of phosphorylation of myosin regulatory light chain in HeLa cells. *Cell Motil. Cytoskeleton* **58**, 186-199.

Buchsbaum, R. J., Connolly, B. A. and Feig, L. A. (2002). Interaction of Rac exchange factors Tiam1 and Ras-GRF1 with a scaffold for the p38 mitogen-activated protein kinase cascade. *Mol. Cell. Biol.* **22**, 4073-4085.

Buchsbaum, R. J., Connolly, B. A. and Feig, L. A. (2003). Regulation of p70 S6 kinase by complex formation between the Rac guanine nucleotide exchange factor (Rac-GEF) Tiam1 and the scaffold spinophilin. *J. Biol. Chem.* **278**, 18833-18841.

Chan, A. Y., Coniglio, S. J., Chuang, Y. Y., Michaelson, D., Knaus, U. G., Philips, M. R. and Symons, M. (2005). Roles of the Rac1 and Rac3 GTPases in human tumor cell invasion. *Oncogene* **24**, 7821-7829.

Chew, T. L., Masaracchia, R. A., Goeckeler, Z. M. and Wysolmerski, R. B. (1998). Phosphorylation of non-muscle myosin II regulatory light chain by p21-activated kinase (gamma-PAK). *J. Muscle Res. Cell Motil.* **19**, 839-854.

Choi, C. K., Vicente-Manzanares, M., Zareno, J., Whitmore, L. A., Mogilner, A. and Horwitz, A. R. (2008). Actin and alpha-actinin orchestrate the assembly and maturation of nascent adhesions in a myosin II motor-independent manner. *Nat. Cell Biol.* **10**, 1039-1050.

Chrzanowska-Wodnicka, M. and Burridge, K. (1996). Rho-stimulated contractility drives the formation of stress fibers and focal adhesions. *J. Cell Biol.* **133**, 1403-1415.

Clark, K., Langeslag, M., Figdor, C. G. and van Leeuwen, F. N. (2007). Myosin II and mechanotransduction: a balancing act. *Trends Cell Biol.* **17**, 178-186.

Dembo, M. and Wang, Y. L. (1999). Stresses at the cell-to-substrate interface during locomotion of fibroblasts. *Biophys. J.* **76**, 2307-2316.

Even-Ram, S., Doyle, A. D., Conti, M. A., Matsumoto, K., Adelstein, R. S. and Yamada, K. M. (2007). Myosin IIA regulates cell motility and actomyosin-microtubule crosstalk. *Nat. Cell Biol.* **9**, 299-309.

Gao, Y., Dickerson, J. B., Guo, F., Zheng, J. and Zheng, Y. (2004). Rational design and characterization of a Rac GTPase-specific small molecule inhibitor. *Proc. Natl. Acad. Sci. USA* **101**, 7618-7623.

Gardel, M. L., Sabass, B., Ji, L., Danuser, G., Schwarz, U. S. and Waterman, C. M. (2008). Traction stress in focal adhesions correlates biphasically with actin retrograde flow speed. *J. Cell Biol.* **183**, 999-1005.

Goeckeler, Z. M., Masaracchia, R. A., Zeng, Q., Chew, T. L., Gallagher, P. and Wysolmerski, R. B. (2000). Phosphorylation of myosin light chain kinase by p21-activated kinase PAK2. *J. Biol. Chem.* **275**, 18366-18374.

Hamann, M. J., Lubking, C. M., Luchini, D. N. and Billadeau, D. D. (2007). Asef2 functions as a Cdc42 exchange factor and is stimulated by the release of an autoinhibitory module from a concealed C-terminal activation element. *Mol. Cell. Biol.* **27**, 1380-1393.

Huttenlocher, A. and Horwitz, A. R. (2011). Integrins in cell migration. *Cold Spring Harb. Perspect. Biol.* **3**, a005074.

Hynes, R. O. (1992). Integrins: versatility, modulation, and signaling in cell adhesion. *Cell* **69**, 11-25.

Ikebe, M. (1989). Phosphorylation of a second site for myosin light chain kinase on platelet myosin. *Biochemistry* **28**, 8750-8755.

Itoh, R. E., Kurokawa, K., Ohba, Y., Yoshizaki, H., Mochizuki, N. and Matsuda, M. (2002). Activation of rac and cdc42 video imaged by fluorescent resonance energy transfer-based single-molecule probes in the membrane of living cells. *Mol. Cell. Biol.* **22**, 6582-6591.

Katoh, K., Kano, Y., Amano, M., Onishi, H., Kaibuchi, K. and Fujiwara, K. (2001). Rho-kinase—mediated contraction of isolated stress fibers. *J. Cell Biol.* **153**, 569-584.

Kawasaki, Y., Sagara, M., Shibata, Y., Shirouzu, M., Yokoyama, S. and Akiyama, T. (2007). Identification and characterization of Asef2, a guanine-nucleotide exchange factor specific for Rac1 and Cdc42. *Oncogene* **26**, 7620-267.

Kiosses, W. B., Daniels, R. H., Otey, C., Bokoch, G. M. and Schwartz, M. A. (1999). A role for p21-activated kinase in endothelial cell migration. *J. Cell Biol.* **147**, 831-844.

Kovács, M., Tóth, J., Hetényi, C., Málnási-Csizmadia, A. and Sellers, J. R. (2004). Mechanism of blebbistatin inhibition of myosin II. *J. Biol. Chem.* **279**, 35557-35563.

Lauffenburger, D. A. and Horwitz, A. F. (1996). Cell migration: a physically integrated molecular process. *Cell* **84**, 359-369.

Laukaitis, C. M., Webb, D. J., Donais, K. and Horwitz, A. F. (2001). Differential dynamics of alpha 5 integrin, paxillin, and alpha-actinin during formation and disassembly of adhesions in migrating cells. *J. Cell Biol.* **153**, 1427-1440.

Liu, Z., van Grunsven, L. A., Van Rossen, E., Schroyen, B., Timmermans, J. P., Geerts, A. and Reynaert, H. (2010). Blebbistatin inhibits contraction and accelerates migration in mouse hepatic stellate cells. *Br. J. Pharmacol.* **159**, 304-315.

Lo, C. M., Buxton, D. B., Chua, G. C., Dembo, M., Adelstein, R. S. and Wang, Y. L. (2004). Nonmuscle myosin IIb is involved in the guidance of fibroblast migration. *Mol. Biol. Cell* **15**, 982-989.

Luque, A., Gómez, M., Puzon, W., Takada, Y., Sánchez-Madrid, F. and Cabañas, C. (1996). Activated conformations of very late activation integrins detected by a group of antibodies (HUTS) specific for a novel regulatory region (355-425) of the common beta 1 chain. *J. Biol. Chem.* **271**, 11067-11075.

Matsumura, F., Ono, S., Yamakita, Y., Totsukawa, G. and Yamashiro, S. (1998). Specific localization of serine 19 phosphorylated myosin II during cell locomotion and mitosis of cultured cells. *J. Cell Biol.* **140**, 119-129.

Niggli, V., Schmid, M. and Nievergelt, A. (2006). Differential roles of Rho-kinase and myosin light chain kinase in regulating shape, adhesion, and migration of HT1080 fibrosarcoma cells. *Biochem. Biophys. Res. Commun.* **343**, 602-608.

Nobes, C. D. and Hall, A. (1995). Rho, rac, and cdc42 GTPases regulate the assembly of multimolecular focal complexes associated with actin stress fibers, lamellipodia, and filopodia. *Cell* **81**, 53-62.

Pawson, T. (2007). Dynamic control of signaling by modular adaptor proteins. *Curr. Opin. Cell Biol.* **19**, 112-116.

Reddy-Alla, S., Schmitt, B., Birkenfeld, J., Eulenburg, V., Dutertre, S., Böhringer, C., Götz, M., Betz, H. and Papadopoulos, T. (2010). PH-domain-driven targeting of collybistin but not Cdc42 activation is required for synaptic gephyrin clustering. *Eur. J. Neurosci.* **31**, 1173-1184.

Ren, X. D., Kiosses, W. B. and Schwartz, M. A. (1999). Regulation of the small GTP-binding protein Rho by cell adhesion and the cytoskeleton. *EMBO J.* **18**, 578-585.

Ridley, A. J. (2001). Rho GTPases and cell migration. *J. Cell Sci.* **114**, 2713-2722.

Ridley, A. J. and Hall, A. (1992). The small GTP-binding protein rho regulates the assembly of focal adhesions and actin stress fibers in response to growth factors. *Cell* **70**, 389-399.

Ridley, A. J., Schwartz, M. A., Burridge, K., Firtel, R. A., Ginsberg, M. H., Borisy, G., Parsons, J. T. and Horwitz, A. R. (2003). Cell migration: integrating signals from front to back. *Science* **302**, 1704-1709.

Rottner, K., Hall, A. and Small, J. V. (1999). Interplay between Rac and Rho in the control of substrate contact dynamics. *Curr. Biol.* **9**, 640-648.

Sabass, B., Gardel, M. L., Waterman, C. M. and Schwarz, U. S. (2008). High resolution traction force microscopy based on experimental and computational advances. *Biophys. J.* **94**, 207-220.

Sagara, M., Kawasaki, Y., Iemura, S. I., Natsume, T., Takai, Y. and Akiyama, T. (2009). Asef2 and Neurabin2 cooperatively regulate actin cytoskeletal organization and are involved in HGF-induced cell migration. *Oncogene* **28**, 1357-1365.

Saito, T., Jones, C. C., Huang, S., Czech, M. P. and Pilch, P. F. (2007). The interaction of Akt with APPL1 is required for insulin-stimulated Glut4 translocation. *J. Biol. Chem.* **282**, 32280-32287.

Sanders, L. C., Matsumura, F., Bokoch, G. M. and de Lanerolle, P. (1999). Inhibition of myosin light chain kinase by p21-activated kinase. *Science* **283**, 2083-2085.

Scholey, J. M., Taylor, K. A. and Kendrick-Jones, J. (1980). Regulation of non-muscle myosin assembly by calmodulin-dependent light chain kinase. *Nature* **287**, 233-235.

Straight, A. F., Cheung, A., Limouze, J., Chen, I., Westwood, N. J., Sellers, J. R. and Mitchison, T. J. (2003). Dissecting temporal and spatial control of cytokinesis with a myosin II Inhibitor. *Science* **299**, 1743-1747.

Tovell, V. E., Dahlmann-Noor, A. H., Khaw, P. T. and Bailly, M. (2011). Advancing the treatment of conjunctival scarring: a novel ex vivo model. *Arch. Ophthalmol.* **129**, 619-627.

Vernon, R. B. and Gooden, M. D. (2002). An improved method for the collagen gel contraction assay. *In Vitro Cell. Dev. Biol. Anim.* **38**, 97-101.

Vicente-Manzanares, M. and Horwitz, A. R. (2011). Cell migration: an overview. *Methods Mol. Biol.* **769**, 1-24.

Vicente-Manzanares, M., Webb, D. J. and Horwitz, A. R. (2005). Cell migration at a glance. *J. Cell Sci.* **118**, 4917-4919.

Vicente-Manzanares, M., Zareno, J., Whitmore, L., Choi, C. K. and Horwitz, A. F. (2007). Regulation of protrusion, adhesion dynamics, and polarity by myosins IIA and IIB in migrating cells. *J. Cell Biol.* **176**, 573-580.

Wang, A., Ma, X., Conti, M. A. and Adelstein, R. S. (2011). Distinct and redundant roles of the non-muscle myosin II isoforms and functional domains. *Biochem. Soc. Trans.* **39**, 1131-1135.

Webb, D. J., Donais, K., Whitmore, L. A., Thomas, S. M., Turner, C. E., Parsons, J. T. and Horwitz, A. F. (2004). FAK-Src signalling through paxillin, ERK and MLCK regulates adhesion disassembly. *Nat. Cell Biol.* **6**, 154-161.

Wegner, A. M., Nebhan, C. A., Hu, L., Majumdar, D., Meier, K. M., Weaver, A. M. and Webb, D. J. (2008). N-wasp and the arp2/3 complex are critical regulators of actin in the development of dendritic spines and synapses. *J. Biol. Chem.* **283**, 15912-15920.

Welf, E. S., Naik, U. P. and Ogunnaike, B. A. (2012). A spatial model for integrin clustering as a result of feedback between integrin activation and integrin binding. *Biophys. J.* **103**, 1379-1389.

Wheeler, A. P. and Ridley, A. J. (2004). Why three Rho proteins? RhoA, RhoB, RhoC, and cell motility. *Exp. Cell Res.* **301**, 43-49.

Wirth, A., Schroeter, M., Kock-Hauser, C., Manser, E., Chalovich, J. M., De Lanerolle, P. and Pfitzer, G. (2003). Inhibition of contraction and myosin light chain phosphorylation in guinea-pig smooth muscle by p21-activated kinase 1. *J. Physiol.* **549**, 489-500.

Yeung, T., Georges, P. C., Flanagan, L. A., Marg, B., Ortiz, M., Funaki, M., Zahir, N., Ming, W., Weaver, V. and Janmey, P. A. (2005). Effects of substrate stiffness on cell morphology, cytoskeletal structure, and adhesion. *Cell Motil. Cytoskeleton* **60**, 24-34.

Zeng, Q., Lagunoff, D., Masaracchia, R., Goeckeler, Z., Côté, G. and Wysolmerski, R. (2000). Endothelial cell retraction is induced by PAK2 monophosphorylation of myosin II. *J. Cell Sci.* **113**, 471-482.

Zhang, H. and Macara, I. G. (2008). The PAR-6 polarity protein regulates dendritic spine morphogenesis through p190 RhoGAP and the Rho GTPase. *Dev. Cell* **14**, 216-226.

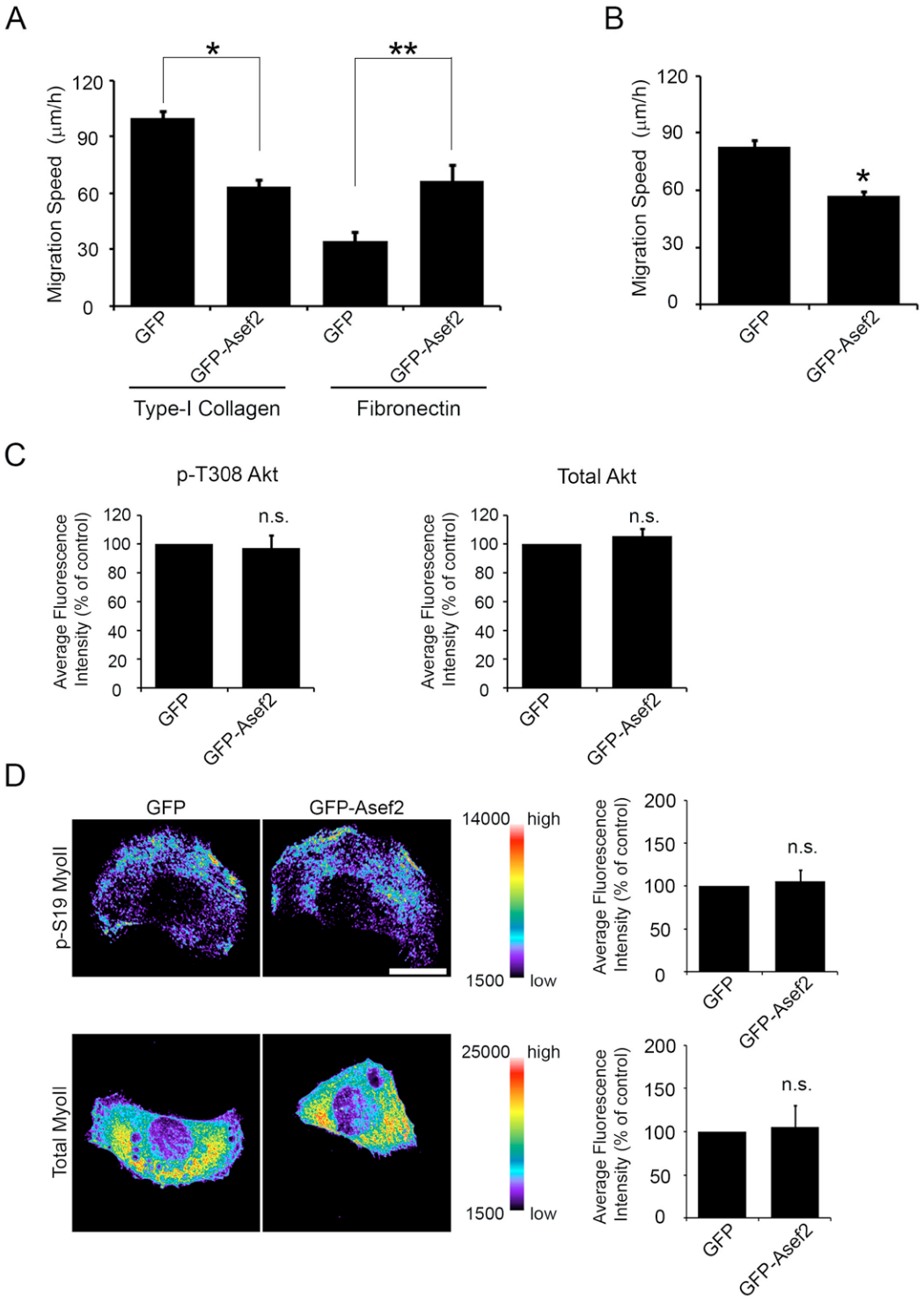

Fig. S1. Asef2 regulates migration on fibronectin and type I collagen through distinct molecular mechanisms. (A) GFP and GFP-Asef2 stable HT1080 cells were plated on fibronectin or type I collagen-coated tissue culture dishes and imaged using time-lapse microscopy. The migration of individual cells was tracked and analyzed. Quantification of the migration speed for cells plated on fibronectin and type I collagen is shown. Error bars represent S.E.M. for at least 59 cells from three independent experiments (*$p < 0.0001$, **$p < 0.007$). (B) Wild-type HT1080 cells were transiently transfected with GFP or GFP-Asef2 and used in migration assays. Quantification of the migration speed for GFP and GFP-Asef2 expressing cells is shown. Error bars represent S.E.M. for at least 49 cells from three independent experiments (*$p < 0.0001$). (C) GFP and GFP-Asef2 stable HT1080 cells were plated on type I collagen-coated glass coverslips and immunostained for Akt phosphorylated at T308 (p-T308 Akt) or total Akt. Right, quantification of the amount of p-T308 Akt (left panel) and total Akt (right panel) in GFP and GFP-Asef2 cells is shown. Error bars represent S.E.M. for at least 30 cells from at least three separate experiments. (D) Left, GFP and GFP-Asef2 stable HT1080 cells were plated on fibronectin-coated glass coverslips and immunostained for MyoII phosphorylated at S19 (p-S19 MyoII) or total MyoII. p-S19 MyoII and total MyoII images are shown in pseudo-color coding. Scale bar: 15 μm. Right, quantification of the amount of p-S19 MyoII (upper panel) and total MyoII (lower panel) in GFP and GFP-Asef2 cells is shown. Error bars represent S.E.M. for at least 55 cells from three independent experiments. For panels C and D, "n.s." denotes no statistically significant difference.

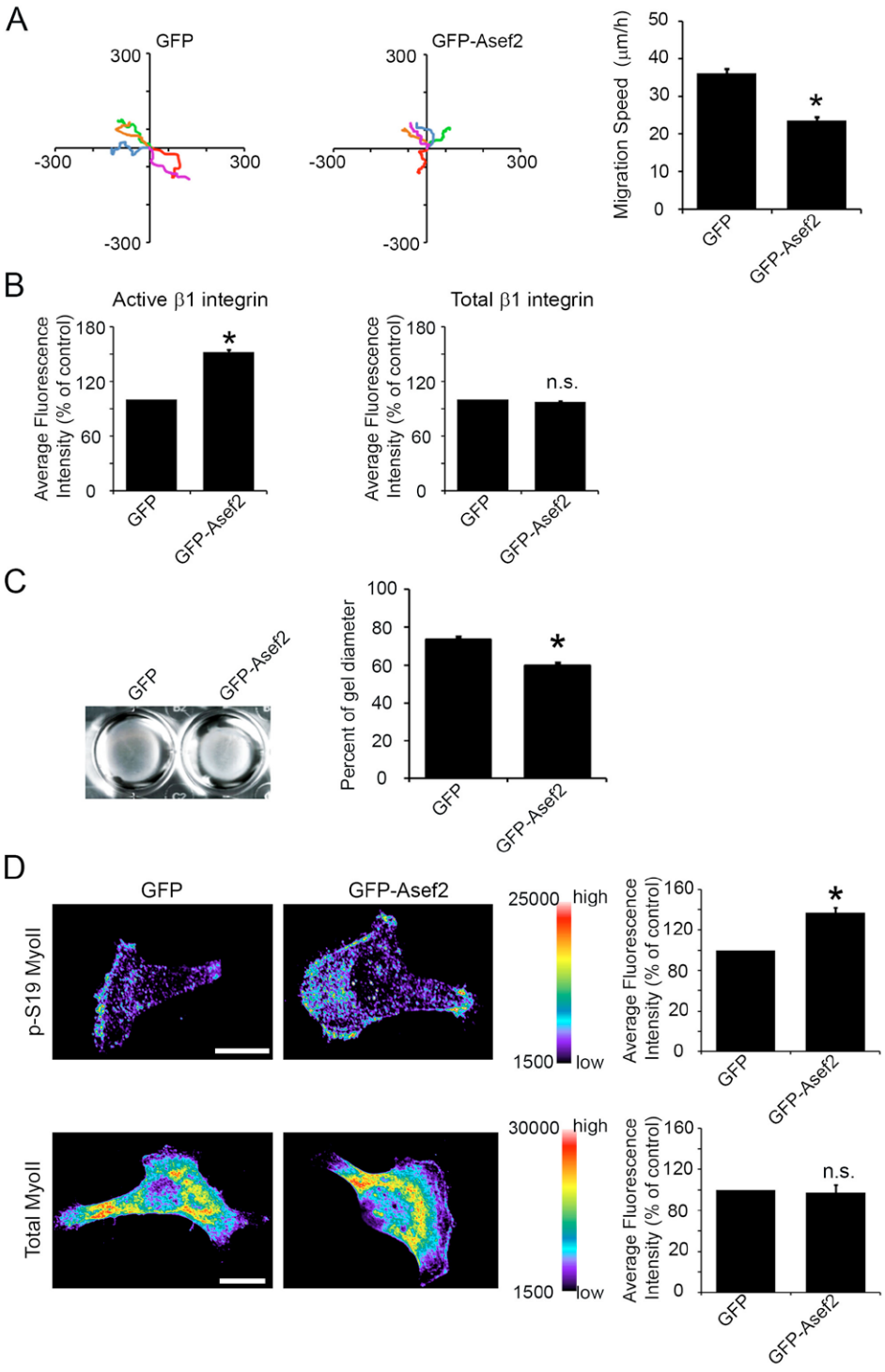

Fig. S2. Asef2 increases the amount of active MyoII and β1 integrin in MDA-MB-231 cells to regulate migration and contractility. (A) GFP and GFP-Asef2 stable MDA-MB-231 cells were plated on type I collagen-coated tissue culture dishes and used in migration assays. Left, Rose plots of migration tracks for five GFP and GFP-Asef2 expressing cells are shown. Right, quantification of the migration speed for GFP and GFP-Asef2 cells is shown. Error bars represent S.E.M. for at least 62 cells from three separate experiments (*$p < 0.0001$). (B) GFP and GFP-Asef2 stable MDA-MB-231 cells, plated on type I collagen, were immunostained for active or total β1 integrin and were imaged with TIRF microscopy. Quantification of the amount of active (left panel) and total (right panel) β1 integrin in adhesions in GFP and GFP-Asef2 cells is shown. Error bars represent S.E.M. from at least 83 adhesions from three independent experiments (*$p < 0.0001$). (C) GFP and GFP-Asef2 stable MDA-MB-231 cells were used in type I collagen gel contraction assays. Left, images of contracted gels with GFP and GFP-Asef2 cells are shown. Right, quantification of gel contraction for GFP and GFP-Asef2 is shown. Error bars represent S.E.M. from three independent experiments (*$p < 0.0009$). (D) Left, GFP and GFP-Asef2 stable MDA-MB-231 cells were plated on type I collagen-coated coverslips and were immunostained for phospho-S19 MyoII (p-S19 MyoII) or total MyoII. p-S19 MyoII and total MyoII images are shown in pseudo-color coding. Scale bar: 15 μm. Right, quantification of the amount of p-S19 MyoII and total MyoII in GFP and GFP-Asef2 cells is shown. Error bars represent S.E.M. for at least 30 cells from three separate experiments (*$p = 0.0002$). For panels B and D, "n.s." denotes no statistically significant difference.

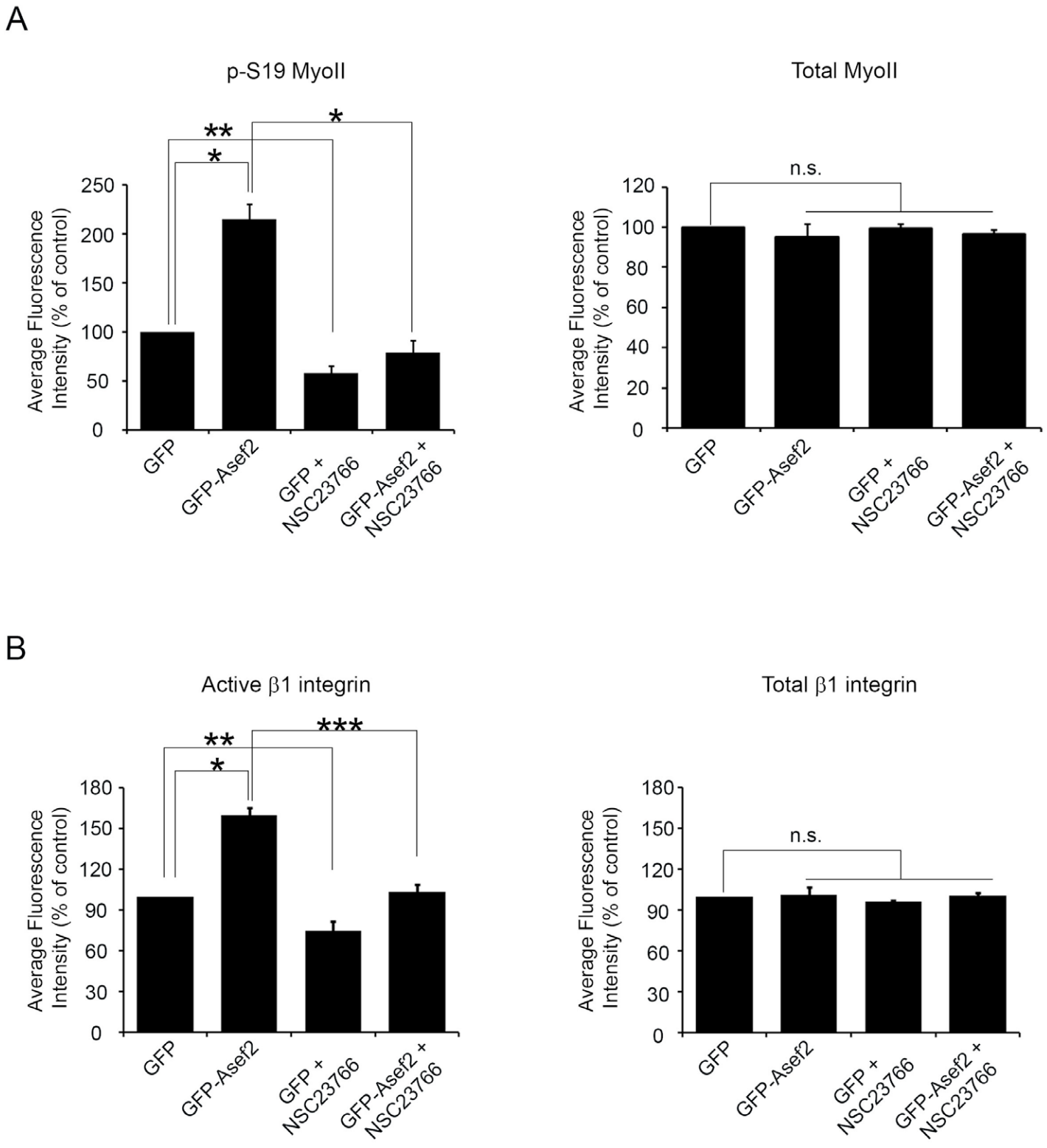

Fig. S3. Asef2 regulates the levels of active MyoII and β1 integrin through Rac. (A) GFP and GFP-Asef2 stable HT1080 cells were treated with the Rac inhibitor NSC23766 or DMSO and were immunostained with antibodies that recognize S19 phosphorylated MyoII (p-S19 MyoII) or total MyoII. Quantification of the amount of p-S19 Myo II (left panel) and total MyoII (right panel) in GFP and GFP-Asef2 cells is shown. Error bars represent S.E.M. for 40 cells from three individual experiments (*$p < 0.002$; **$p < 0.006$). (B) GFP and GFP-Asef2 stable HT1080 cells were treated with the Rac inhibitor NSC23766 or DMSO, immunostained for active or total β1 integrin, and imaged with TIRF microscopy. Quantification of the amount of active (left panel) and total (right panel) β1 integrin in adhesions in GFP and GFP-Asef2 cells is shown. Error bars represent S.E.M. from at least 56 adhesions from three separate experiments (*$p = 0.0004$; **$p < 0.03$; ***$p < 0.003$). "n.s." denotes no statistically significant difference.

Movie 1. Migration of GFP stable HT1080 cells. This movie corresponds to Fig. 1A. Images were collected every 5 min for 180 min using phase microscopy.

Movie 2. Migration of GFP-Asef2 HT1080 stable cells. This movie corresponds to Fig. 1A. Images were collected every 5 min for 180 min using phase microscopy.

Movie 3. Migration of wild-type HT1080 cells transfected with a non-targeting shRNA. This movie corresponds to Fig. 1C. Images were collected every 5 min for 180 min using phase microscopy.

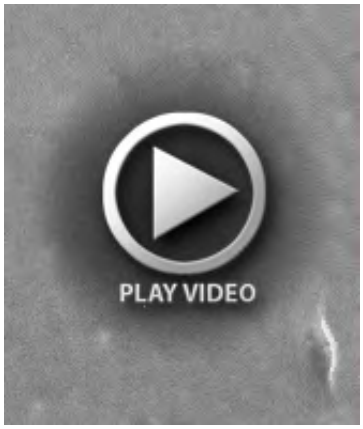

Movie 4. Migration of wild-type HT1080 cells transfected with Asef2 shRNA 1. This movie corresponds to Fig. 1C. Images were collected every 5 min for 180 min using phase microscopy.